SINTERING AND GRAIN GROWTH OF NONSTOICHIOMETRIC RUTILE

BY

JACQUES PIERRE JEAN THIRIAR

A THESIS SUBMITTED IN PARTIAL FULFILMENT OF

THE REQUIREMENTS FOR THE DEGREE OF

MASTER OF APPLIED SCIENCE

in the Department

of

METALLURGY

We accept this thesis as conforming to the

standard required from candidates for the

degree of MASTER OF APPLIED SCIENCE.

Members of the Department of Metallurgy

THE UNIVERSITY OF BRITISH COLUMBIA

February 1964

In presenting this thesis in partial fulfilment of the requirements for an advanced degree at the University of British Columbia, I agree that the Library shall make it freely available for reference and study. I further agree that permission for extensive copying of this thesis for scholarly purposes may be granted by the Head of my Department or by his representatives. It is understood that copying or publication of this thesis for financial gain shall not be allowed without my written permission.

Department of Metallurgy.

The University of British Columbia,
Vancouver 8, Canada.

Date February 28th, 1964

ABSTRACT

Rutile powders in flaked form were pressed and heated at different temperatures (1000°C to 1300°C) under reducing (H_2/H_2O) atmospheres to study the rate of weight loss, the grain growth and the densification.

The weight loss measurements for reduction of rutile to two non-stoichiometric compositions of $TiO_{1.92}$ and $TiO_{1.98}$ yielded an activation energy for weight loss of 82 ± 2 kcal/mole. No attempt was made to identify the rate-determining step. Previous weight loss measurements carried out in equilibrium conditions produced an enthalpy of 83 ± 10 kcal/mole for the formation of an oxygen ion vacancy. This could suggest that the rate-determining step might be the formation of an oxygen ion vacancy.

The grain growth study revealed that the non-stoichiometric composition of $TiO_{1.92}$ did not obey the theoretical relation of Burke. The results can be expressed by the following

$$D^2 - D_o^2 = K\, t^{0.6} \exp\left(-\frac{78{,}000}{RT}\right)$$

This activation energy for grain growth is equal to the activation energy for oxygen ion diffusion in TiO_2. This suggests that the oxygen ion diffusion may be the rate-controlling step for grain growth.

The densification on sintering was evaluated from linear shrinkage measurements of the compacts during reduction to $TiO_{1.92}$. A few models were tried, to find the best fit for the present data. While the photomicrographs suggest the Coble model for bulk diffusion, and the values for the diffusion coefficients are of the right order of magnitude, the activation energy for the rate determining step is about 118 kcal/mole, which is not in agreement with the previous sintering study on rutile.

From grain growth data for those compacts reduced to $TiO_{1.98}$ at 1200°C and those sintered in open air, it was seen that the diffusion coefficient was not significantly affected by variation of the oxygen partial pressure. This discrepancy in the activation energy value may be explained by a possible error in measurement and other unknown variables which may control the densification process.

ACKNOWLEDGEMENT

The author wishes to gratefully acknowledge the assistance given by members of the Department of Metallurgy. He is especially grateful to Dr. A. C D. Chaklader for his advice, guidance and assistance and to Mrs. A. M. Armstrong for her critical discussions in the preparation of the thesis.

The work was financed by a grant provided by the Defence Research Board of Canada, D.R.B. 7501-02.

TABLE OF CONTENTS

Table of Contents Continued...

LIST OF FIGURES

List of Figures Continued...

LIST OF TABLES

INTRODUCTION

Because of the very high melting temperature of most oxide ceramics, densification by sintering of powder compacts is a common fabrication technique. Although this technology may be as old as the arts of ceramics, an understanding of the mechanisms involved during the sintering processes is only a recent development.

The term "sintering" as used by the powder metallurgists, means an operation by which a mass of compacted powder is transformed into a more dense product by the application of heat alone. Observation of the increased cohesion between the particles suggests that the process may be divided into stages. In the first stage, the growth of bridges between adjacent particles occurs, but with very little densification. In the subsequent stages, the interparticle necks grow bigger producing a noticeable shrinkage. Further neck growth would result in the formation of isolated pores.

The most successful determinations of the kinetics of sintering have been made utilizing systems of simplified geometry, where the study of the neck growth is quite feasible by simple experimental techniques. For this reason, experiments in this field have been mostly confined to the measurement of the rate of neck growth between a sphere and a plane, between two spheres, between a wire and a plane or between two wires as a function of time and temperature. Such systems have the distinct advantage that their geometry is well known, but they have limited applicability to the densification of powder compacts.

Earlier Theories of Sintering (Spherical Models)

Kuczynski[1] was the first to attempt to derive the rate expressions for the growth of the neck at the point of contact between two spherical particles. According to him, the first stage of sintering may be characterized by the formation of a neck between two particles as shown in Figure 1.

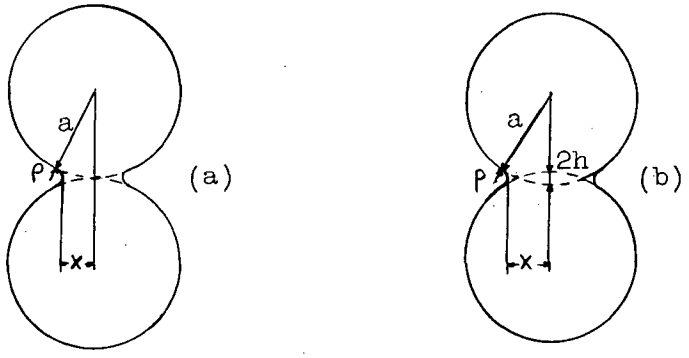

Figure 1. Schematic Representation of the Contact Area Between Two Partially Sintered Spheres.

(a) Center-to-center distance constant,

(b) Center-to-center distance shrinks, (after Kuczynski[1]).

This can be brought about by one or more of the following processes: the viscous or plastic flow; evaporation and condensation; and volume or surface diffusion. The well-known relationship between the radii x of the neck and a, of the spheres, time t, and temperature T can be described by one general equation

$$\frac{x^n}{a^m} = F(T)t \qquad \ldots\ldots(1)$$

where F (T) is a function of temperature only.

The different mechanisms involved in the sintering process are related by the following numerical values:

$n = 2$	$m = 1$	for viscous or plastic flow
$n = 3$	$m = 1$	for evaporation and condensation
$n = 5$	$m = 2$	for volume diffusion
$n = 7$	$m = 3$	for surface diffusion.

Although it has been recognized that the decrease of total surface energy of the compacts is a motivating force for sintering, this excess surface energy in actual compacts has never been very great. For instance, the net decrease in free energy occuring on sintering a 1 μ particle size material corresponds to an energy decrease of about 1 cal/gm. However, in the neck area there exist stresses due to the curvature which may produce mass flow or a lowering of the vapour pressure in the neck region. The vapour pressure over a flat surface p_o and Δp, the lowering of the vapour pressure due to the radius of curvature p, are related by the following expression, first derived by Kelvin[2]

$$\frac{\Delta p}{p_o} = - \frac{\gamma V_\Theta}{RTp} \qquad \ldots\ldots(2)$$

where γ is the surface energy and V_Θ the molar volume of the solid. The evaporation-condensation mechanism for material transport during sintering can be easily understood from this relationship. If the vapour pressure over the flat surface (or over the convex surface in the spherical model, Figure 1) is higher than that of the neck region (radius p), particularly at high temperatures, evaporation from the convex region and subsequent condensation in the cavity of the neck can be expected to occur, resulting in neck growth.

Another consequence of the existence of the stresses in the neck can be determined by considering the vacuum surrounding the neck as a fluid composed of vacancies which evaporate into the solid. For these vacancies, the cavity of the neck will be a convexity and consequently the pressure of vacancies in the neck area will be greater than under the surfaces of the other parts. Assuming that the vacancy pressure is proportional to their concentration in the solid, equation (2) may be rewritten as

$$\frac{\Delta C}{C_6} = \frac{\gamma V_o}{RTp} \qquad \ldots\ldots(3)$$

where C_o is the equilibrium vacancy concentration under a flat surface. Due to the excess concentration of vacancies ΔC in the neck area, there exists a gradient of vacancies between this area and the interior of the system. This will result in the vacancy migration along their gradient accompanied by the volume or surface diffusion of atoms in the opposite direction. The excess of vacancies have to be removed from the system by depositing them at the possible sinks, which may be the nearby surface or the grain boundaries. The vacancies deposited in the grain boundaries can either be diffused rapidly to the solid vapour interface, because the rate of diffusion is much larger in the grain boundary than in the bulk of the body; or if the fluidity of the material in the grain boundary is high (as in the case of the viscous flow) the vacancies will collapse, as any void will in a liquid of low viscosity. In any case, the elimination of vacancies via grain boundaries will result in the shrinkage accompanied by center-to-center approach of the particles. On the other hand, if the elimination of vacancies occurs at the free surface, the center-to-center distance of the spheres will not change as would be the case in densification

by the evaporation and condensation mechanism.

From the derived expression for ΔC, equation (3) and by using the first Fick's diffusion equation, the equation for volume diffusion mechanism can be obtained. Its final form is

$$\frac{x^5}{a^2} = \frac{K \gamma V_o}{RT} D_v t \qquad .....(4)$$

where D_v is the volume self-diffusion coefficient; K is a numerical constant and has a value of about 100.

Densification of Powder Compacts

The increase in density of a powder compact during sintering is of the greatest practical importance, but due to the number of unknown variables or poorly defined parameters involved in the sintering process, it is difficult to evaluate the basic mechanisms of material transport. The earlier measurements of powder compacts consisted mostly of determining their density as a function of temperature, although the time variable is of great significance from the point of view of the kinetics of the process.

Kingery and Berg[3] tried to apply the volume diffusion equation for neck growth between two particles to powder compacts of oxides. They assumed that the volume of the neck at any time is equal to the volume of the pore space removed from the system, and obtained the following relationship by using equation (4)

$$\frac{\Delta V}{V_o} = -\frac{3n}{8} \left[\frac{40 \gamma V_o D_v}{a^3 k T} \right]^{4/5} t^{4/5} \qquad .....(5)$$

where ΔV and V_o are the change of volume with time and initial

volume respectively, n is the number of points of contact determined by the coordination state of the particles. From the experimental observations they have found that this equation has very limited applicability. Although it can be applied for a volume shrinkage of up to 2%, it failed completely for a shrinkage greater than 6%. Kuczynski[4] approached the problems of densification of compacts from the point of view of pore shrinkage and considered two possible mechanisms for material transport into the pores: viscous or plastic flow and volume diffusion.

The End-Point Density

Earlier studies on densification of powdered metals and oxides indicated that it was not possible to reach the theoretical density by sintering alone and this led the powder metallurgists to believe that there is an "end-point density" for all materials.

In a recent study, Coble[5] showed that the end-point density is the result of grain growth, which takes place simultaneously during sintering. He postulated a model and derived an equation to support this hypothesis that as long as the grain growth is continuous and the pores are connected by the grain boundaries, complete elimination of pores in the boundaries can be achieved, and this will result in complete densification. Only when discontinuous grain growth took place in a system would the pores be trapped inside the grains. These trapped pores would not shrink any further. In the latter case, the powder compact would reach an end-point density which would be below the theoretical limit of densification. Coble, using doped alumina (to control grain growth) showed experimentally that it is possible to achieve theoretical density only by sintering. On the other hand, undoped

Al_2O_3 with its unrestricted grain growth reached an end-point density after a certain period of sintering. This phenomenon of exaggerated grain growth and appearance of trapped pores after a few hours of sintering occurs only at or above a certain temperature called the Sauerwald temperature[6], T_S. This is generally 2/3 to 3/4 of the melting point of the material.

Pore Structure

The change in shape and size of the pores is very difficult to study in real compacts as the pores are of different sizes and shapes. In the first stage, the necks grow between adjacent particles and the grain boundary does not move, because any displacement towards the center of the particle would mean an increase in boundary area and thus, an increase in grain boundary energy. Afterwards, as sintering proceeds and as the vacancy flux is inversely proportional to the pore radius, the larger pores may increase in size as a result of the condensation of vacancies originating from the smaller ones. Thus, the pores may be classified as small ones, which shrink, and large ones, which increase in size, during sintering. The smaller pores are much more numerous and may include the bulk of the porosity in the compact. When they disappear gradually the overall density of the compact increases. On the other hand, the pores of the second group may control the grain growth by anchoring the grain boundaries.

The critical diameter (δ) of the pores of radius r, which is most effective in inhibiting grain growth, and the volume fraction porosity f in the material are related, according to Zener[7] by the following relationship

$$\delta = \frac{4}{3} \frac{r}{f}$$

As soon as the larger pores reach the critical diameter, exaggerated grain growth will occur and the trapped pores will not shrink any more.

Model for Complete Densification

Coble[5] was the first to formulate bulk diffusion models for the total course of shrinkage in powder compacts, leading to theoretically dense products. He assumed that there are three stages of densification. In the initial or first stage, interparticle contact area increased from zero to 0.2 of the cross-sectional area of the particle. This stage, also refered to as the neck growth stage, usually is accompanied by an increase in relative density of powder compacts from 0.5 to 0.6. This is shown in Figures 2a and 2b. During the initial stage of sintering, grain growth can not occur, as it would require migration of the grain boundary from the minimum area position which in turn would result in an increase in area and energy.

In the second or intermediate stage, grain growth begins and pore shape changes to produce a matrix of pores and grain boundary. The equilibrium angles formed between them are dictated by surface tension such that the three interacting surfaces form a spatial force balance. This stage can be represented by Figure 2c. The pore phase is very similar to a continous channel and is assumed to be cylindrical in shape.

The final stage begins when the pore becomes discontinuous and the channels are replaced by the grain boundaries. The pores only occupy the four grain corners and are nearly spherical in shape as shown in Figure 2d. These pores at the four grain corners will gradually shrink to zero size and the sintering will proceed to theoretical density of the compact. An

alternative final stage would be when discontinuous grain growth occurs before all the porosity is removed. In this case complete elimination of pores would be impossible. Coble supported his arguments by comparing his hypothetical model with the microstructures of the specimens at different stages of sintering. These stages are shown in Figure 3.

The final equation relating the rate of pore shrinkage with other parameters has the following form

$$\frac{dP}{dt} = \frac{N D_v \gamma a_o^3}{l^3 k T} \qquad \ldots\ldots(6)$$

where N = numerical constant: for cylindrical pore case N = 10
for closed pore case N = $\frac{6\pi}{\sqrt{2}}$

D_v = bulk diffusion coefficient
γ = surface energy
a_o^3 = vacancy volume
l = average grain diameter
k = Boltzmann's constant
T = absolute temperature

Sintering of Oxides

a) Neck Growth Experiments

To test the kinetics of sintering, (particularly the initial stage) spheres of Al_2O_3, TiO_2 and ZnO have been used by several workers. Kuczynski[8] particularly used spheres of sapphire to test his volume diffusion model of neck growth. Parravano and Norris[9] used spheres of ZnO to study the rate of neck growth as a function of temperature. Their result supported the model of evaporation and condensation for material transport in that system. O'Bryan and Parravano[10] studied the sintering of single crystals of rutile in air and in reducing atmosphere in the temperature range of 900-1350°C, using a sphere-to-sphere model. Their work indicated that the predominant mechanism of material transport for sintering was volume diffusion and they

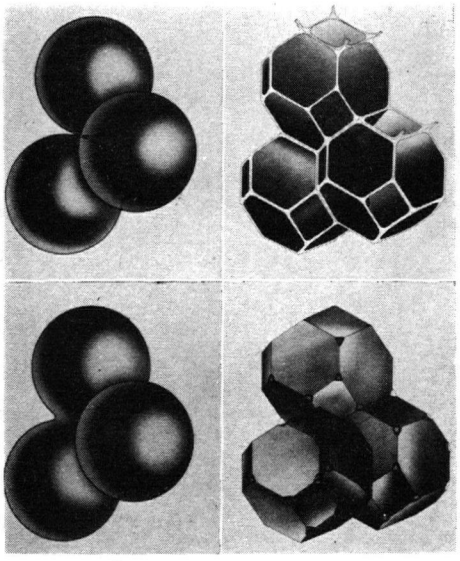

Figure 2. (a) Initial Stage of Sintering, (b) Near End of the Initial Stage; spheres have begun to coalesce. (c) Intermediate Stage; dark grains have adopted shape of tetrakaidecahedron, enclosing white pore channels at grain edges. (d) Final Stage; pores are tetrahedral inclusions at corners where four tetrakaidecahedra meet. (after Coble[5]).

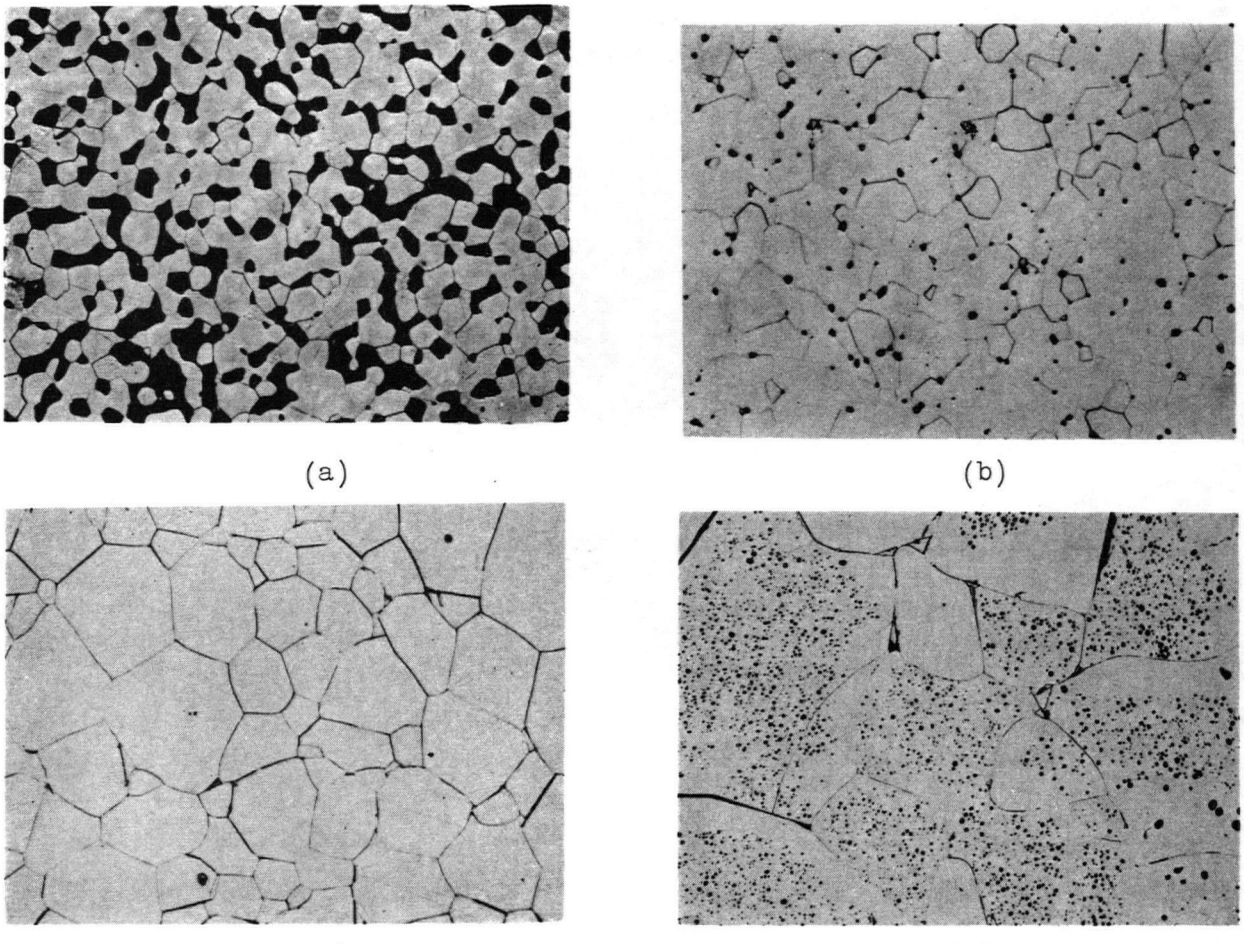

Figure 3. (a) Typical Intermediate Stage Structure
(b) Typical Final Stage Structure
(c) End Stage at Theoretical Density
(d) Final Stage After Discontinuous Grain Growth
(after Coble[5]).

obtained an activation energy of 70 ± 4 kcal/mole for the process. Kawai and Whitmore[11] also independently studied the sphere-to-plate bonding of vacuum-reduced monocrystalline rutile over the temperature range of 1200-1275°C. The rate law governing the interfacial growth indicated also that the volume diffusion was the predominant mechanism of material transport in the sintering process.

b) Densification of Powder Compacts

The densification of powder compacts of oxide was studied by Coble[12] as discussed previously. He used alumina as the standard material to test his hypothesis. Very recently, Johnson and Cutler[13] also carried out investigations on the linear shrinkage rate of alumina powder compacts. Both of these investigations indicated that bulk diffusion, and not the grain boundary diffusion was the basic mechanism of densification. Clark and White[14] used magnesia powder compacts to study the rate of densification and explained their results on the basis of a plastic flow model. The effect of non-stoichiometry on the rate of densification has been studied by several workers[15] with UO_{2+x}.

No results have been reported on the densification of TiO_2 powder compacts, although sintered TiO_2 discs are being widely used in the microwave guide tubes at the present time.

Crystal Structure of Titania[16]

Titanium dioxide can crystallize in three forms. Mineralogically they are known as rutile, anatase and brookite. Rutile is the stable form above 820°C but metastable at room temperature and exists in all commercial titania products.

Rutile has a tetragonal structure with a = 4.4923 Å and c = 2.8930 Å. From a consideration of purely ionic structure, the radius ratio of titanium to oxygen ion predicts a six-fold coordination of titanium with oxygen. The rutile structure may be described as built up from distorted TiO_6 octahedra, the octahedra forming chains in the c-direction and each octahedron sharing an edge with the adjacent members of the chains. The crystal density is 4.26 gm/cm^3, as determined from the X-ray measurements. In the rutile structure titanium and oxygen are present in their highest valence state +4 and -2. Titanium is a transition metal of the iron group and its normal electronic configuration is $(4s)^2(3d)^2$ outside the argon core.

Defect Reaction in Rutile

Straumanis[17] et al. recently measured the density and lattice parameter of rutile powders for the oxygen deficiencies from 0.5 to 0.8 atomic per cent. Their results indicate that the size and shape of the unit cell in this range do not change appreciably so that the change in density can be attributed to oxygen vacancies alone.

Kinetic studies of the oxidation of titanium, under conditions such that rutile is the only oxide in the tarnish layer, did not provide unambiguous information covering either the predominant point defect or the slower moving ionic species in rutile. The investigations of Gulbransen and Andrew[18], and Kinna and Knorr[19] support the case for interstitial cation diffusion being rate-controlling, while those of Birchenall[20], Hauffe[21] and others[22] show oxygen ion diffusion controlling the oxidation of titanium.

From the semi-conducting behaviour of rutile it is well established that rutile becomes a metal excess n-type semi-conductor upon reduction. The predominant point defects are oxygen ion vacancies which are capable of trapping electrons and thereby acting as a donor center.

Aim of the Present Investigation

This present investigation has been mainly concerned with sintering and grain growth of non-stoichiometric titania powder compacts. All the experiments were carried out in a controlled oxygen partial pressure over a temperature range of 1000 to 1250°C. This was to maintain a constant vacancy concentration of oxygen in the system, i.e. a constant ratio of titanium to oxygen in the non-stoichiometric titania.

In addition, the rate of weight loss was also determined in the specimens used for the investigation of sintering and grain growth.

EXPERIMENTAL

Titania Powder

All experiments were performed using rutile powders supplied by the J. J. Baker Chemical Company, Phillipsburg, N. J.

Two one-pound samples were used, the chemical composition of which is given in the following table.

Table I.

Analyses of the Two Rutile Powder Samples

	Lot 21303	Lot 28365
Water Soluble Salts	0.05 %	0.02 %
Arsenic	0.0001	0.00005
Iron	0.002	0.002
Lead	0.008	0.004
Zinc	0.004	0.005

To determine the grain size and shape of the powders, three methods were tried: first, the standard Tyler sieves; second, a sedimentation technique using Andreasen's pipette; and third, measurement of the grain size derived from pictures taken by the electron microscope.

Figures 4 and 5 represent the pictures taken by the electron microscope with the magnification of 3000 and 4000. These show that the grains were flaked, having two large dimensions but little thickness. The particles were all in sub-sieve range. According to the measurements carried out by the Andreasen's pipette technique, over 80 % of the particles are less than 4 microns. The particle size was also determined by taking the average of the particle dimensions in Figures 4 and 5 and is 1.5 μ. The largest and smallest dimensions are 4.25 μ and 0.25 μ respectively.

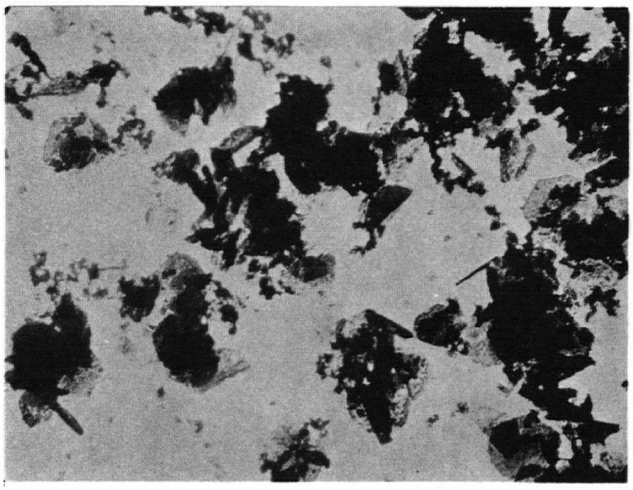

Figure 4. Electron Micrograph of TiO_2 Powders Showing the Size and Shape of the Particles.

X 3000

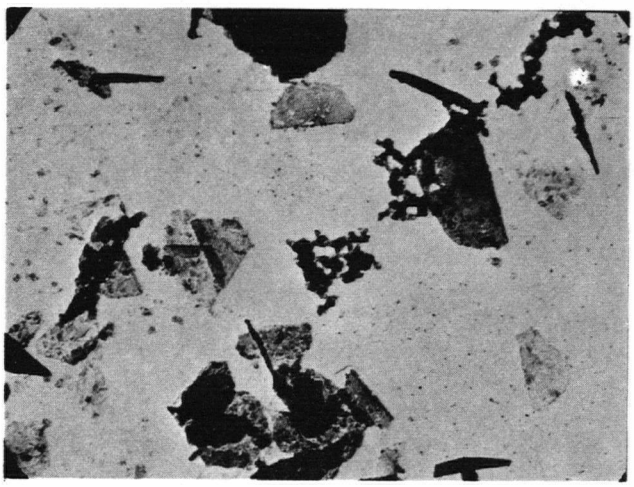

Figure 5. Electron Micrograph of TiO_2 Powders Showing the Size and Shape of the Particles.

X 4000

However, the average grain size of smaller particles, which are the larger fraction, have an average diameter of about 0.8 μ.

Compaction of the Powder

One cylindrical die having an internal diameter of 0.5 inches and another one of rectangular shape, having the internal cross-sectional dimensions of 0.5 X 4 inches were used for compacting the powder. The specimen thickness was kept approximately 0.25 inches because thicker specimens tended to break down during firing. Earlier investigations made on compacting powders of brittle materials, such as oxides, used compacting pressures ranging from 5,000 to 40,000 psi. In the present investigation it was found that an increase of pressure from 7660 to 40,000 psi increased the initial green density of the compacts from 1.93 to 2.30 gm/cm^3. However, as the compacting pressure was increased, laminar cracks appeared on the specimens. These caused the specimens to break into pieces on sintering. As the specimens were also used for weight loss studies, no lubricant of any kind could be used. Therefore, a compacting pressure of 12,000 psi was adopted for all the weight loss, grain growth and sintering measurements.

The Furnace

The furnace used for all experiments was essentially a horizontal type tube furnace heated by four globar heating elements. As shown in Figure 6, the main tube consisted of a long Zircotube of 1 1/8 inches in diameter passing through the heating chamber, which was built with insulating bricks. Both ends of the tube were cooled by circulating water through copper jackets. Thus the specimen, while still inside the furnace was cooled quickly after it was removed from the heating zone. A second Zircotube

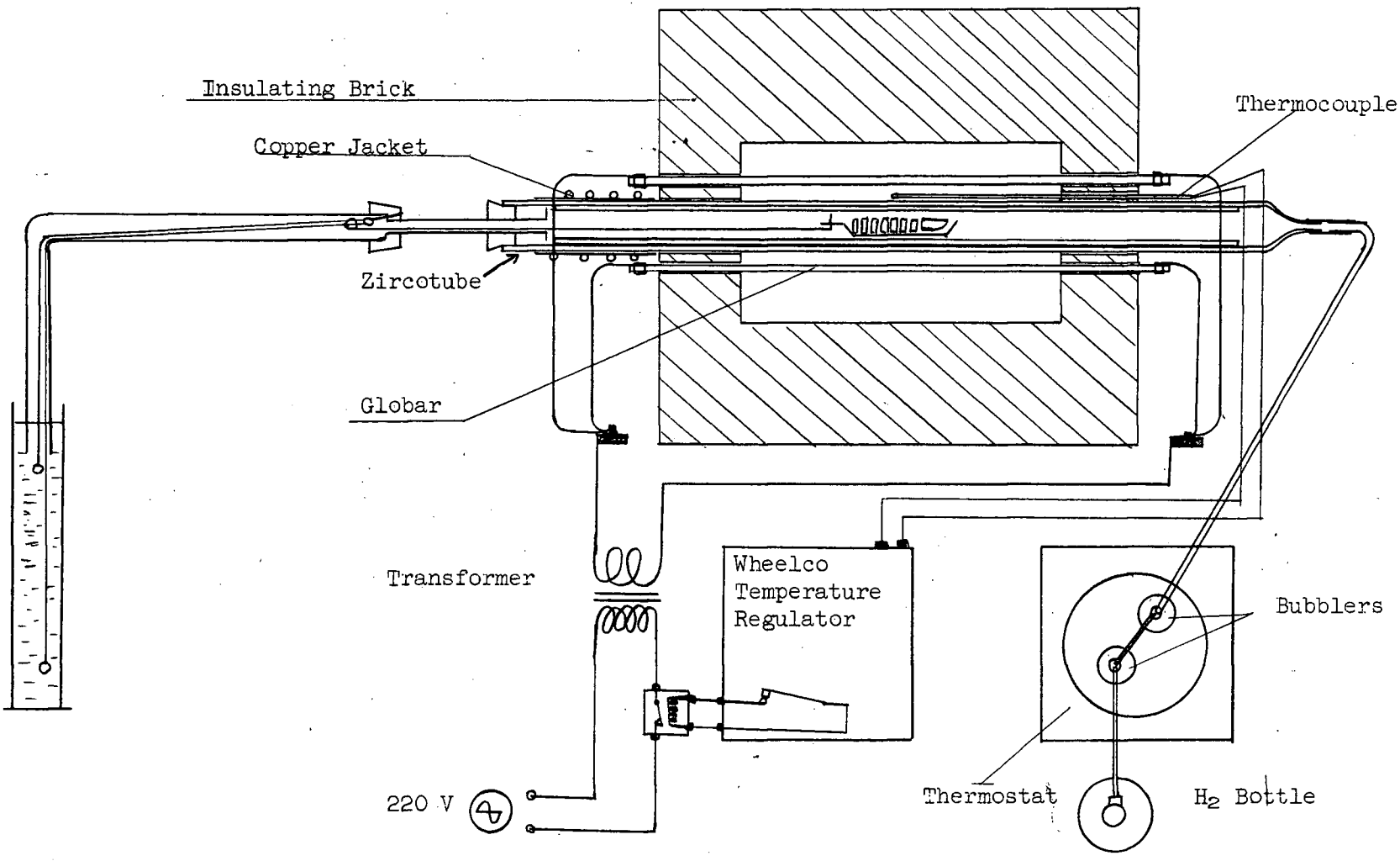

Figure 6. Schematic Diagram of the Furnace

of 0.9 inches internal diameter was fitted inside the main one to avoid any thermal shock on the latter when the hot boat was pulled into the cool zone. The inlet of the tube was connected to a heated copper tube which was joined to a bubbler and which carried reducing atmosphere. The outlet was directly connected to a long glass tube bent at right angles, the end of which was dipped into a water bath. By this arrangement the furnace was essentially a closed system.

With the help of a string system as shown in Figure 6 it was possible to move the boat from the cool zone to the hot zone and vice-versa.

The temperature was measured by the use of a Pt-Pt 10% Rh thermocouple inserted into a protection tube and placed just above the main Zircotube. This thermocouple was connected to a Wheelco temperature regulator which controlled the temperature within ± 10°C.

There was a temperature gradient along the length of the main Zircotube and also a temperature difference between the thermocouple and the specimen. For this reason the position of the boat was maintained in the three inches of hot zone where the temperature was relatively constant and almost equal to the recorded temperature in the Wheelco regulator. The temperature of the specimens was occasionally measured with a separate standardized Pt-Pt 10% Rh thermocouple.

Control of the Furnace Atmosphere

The ratio of the pressures of H_2 and H_2O in the inlet gas of the furnace was determined by passing hydrogen slowly into two bubblers, submerged in a bath of water which was maintained at a fixed temperature. The flow of hydrogen was kept as low as possible to have an equilibrium

atmosphere inside the bubblers. From the early results of reduction it appeared that flows of less than 70 bubbles a minute gave reproducible results.

The bubblers were connected with the furnace by a copper pipe which was heated by a resistance element at a temperature of 70°C, slightly higher than the bath temperature to avoid any condensation.

Description of a Run in the Furnace

The alumina specimen holder was loaded with five to fifteen specimens and was put inside the tube in the cool zone. The furnace atmosphere was gradually changed to the desired atmosphere first by flashing it with a flow of argon for 10 minutes and subsequently by a flow of predetermined H_2/H_2O mixture for 15 minutes. Afterwards the specimens holder was pushed into the hotest zone of the tube. The recorded time for all runs began when the boats were first in the hot zone. After a definite time of firing the reverse procedure was followed. The specimen holder was pulled back into the cooling zone but the same flow was maintained for several minutes to avoid any change in the stoichiometry of rutile. When the specimen temperature was sufficiently low the tube was flashed with argon for 10 minutes and finally the specimens were taken out for measurements.

After the appropriate measurements were taken the specimens were replaced in the boat and the process was repeated.

Measurements for Weight Loss and Dimensional Change

The weight loss and shrinkage measurements were carried out on the same specimens, as both of these measurements were needed to calculate the relative density.

From the weight ratio of titanium to titania which is 47.9/79.9, the weight of titanium in the specimen before reduction was deduced. The weight of the oxygen was determined by subtracting the weight of the titanium from the weight of the initial rutile having a stoichiometric composition of TiO_2. The loss of oxygen after reduction was obtained by subtracting the initial fixed weight of titanium from the weight of the specimen. These measurements were taken on a Christian Beckers manual balance.

The shrinkage was calculated by measuring the length and width of the specimen with a micrometer having an accuracy of ± 0.001 inches. The average of these two linear shrinkages was used to deduce the volume shrinkage from the following relation

$$\frac{\Delta V}{V_o} = \left[1 - \left(1 - \frac{\Delta L}{L_o}\right)^3 \right] \times 100$$

From the weight measurements and from the dimensions of the specimens after different periods of heat treatment, the volume and the bulk densities were calculated and recorded.

Measurements for Grain Growth

a) Polishing and Etching

For the study of grain growth, the specimens were polished first using sandpaper of various sizes and then using wheels having suspensions of fine alumina powder.

The sandpapers used were of the types 1, 0, 00 and 000; the alumina powder had an average grain size of 0.05 μ. When the surfaces of the polished specimens were free from any visible scratches, they were etched by immersing them in a bath of concentrated boiling H_2SO_4 for 2 to

3 minutes. Some specimens were subjected to a thermal etch for three minutes at 650°C before acid etching. This is to make the grain boundaries more apparent. In this case however, the time for the H_2SO_4 immersion was reduced to 30 seconds.

b) Grain Size Measurements

Several pictures of known magnification of these specimens were taken with a Reichert metallographic microscope using reflected light. A magnification of 1500 was used for the specimens having smaller grains whereas a magnification of 600 was used for those having larger grains. The average grain size measurements were made using the intercept (or Heyn) procedure[23].

RESULTS

X-Ray Investigation

To investigate the stability range of rutile on reduction the following preliminary experiment was carried out. Compacts of rutile were reduced to a fixed ratio of titanium to oxygen by heating in the furnace already described and by using different ratios of H_2/H_2O partial pressures over the temperature range of 1000 to 1300°C.

The specimens were scanned in a Norelco X-ray diffractometer for the Bragg angles of 10° to 80°. The "d" values were calculated from the corresponding diffractometric peaks and compared with the standard A.S.T.M. cards for identification of the oxides present. It was established that the rutile was stable up to a non-stoichiometric composition of $TiO_{1.92}$. The compound Ti_3O_5 was detected only in reduced rutile having a composition of $TiO_{1.91}$.

In the same investigation, the relationship between the bubbling rate of H_2 in the water bath and the corresponding equilibrium ratio of titanium to oxygen obtained at the different temperatures was determined.

These ratios were subsequently used during sintering, weight loss and grain growth measurements.

Weight Loss Study

The rates of reduction of TiO_2 to two well defined non-stoichiometric compositions having the rutile structure ($TiO_{1.92} \pm 0.01$ and $TiO_{1.98} \pm 0.01$) were determined by weight loss measurements. These experiments were carried out at 1000, 1050, 1100, 1150 and 1200°C under the appropriate H_2/H_2O

atmospheres to yield these compositions at equilibrium.

The fractional weight loss $\frac{\Delta W}{W}$ of the compacts can be related to the time of reduction by the following type of generalized equation.

$$\frac{\Delta W}{W} = (A\ t)^n \qquad \ldots\ldots(7)$$

ΔW = weight loss at time t
W = original weight
A = a function of temperature, pressure and geometry of the sample.

In order to determine the value of the exponent n, the weight loss data given in Appendix I, Tables1 and 2 were plotted as log $(\frac{\Delta W}{W})$ versus log t. This plot is shown in Figure 7 for $TiO_{1.92}$ and in Figure 8. for $TiO_{1.98}$ as equilibrium products. The slope of the lines produced a value of n = 0.54 ± 0.1 for $TiO_{1.92}$ and n = 0.48 ± 0.01 in the case of $TiO_{1.98}$.

A literature survey[24] revealed that such a reduction process usually follows either a linear or a parabolic law. Therefore the average value of n = 0.52 ± 0.01 suggests a parabolic relation. Equation (7) can then be written as

$$\frac{\Delta W}{W} = (A\ t)^{0.5} \qquad \ldots\ldots(8)$$

The values of the function $A^{0.5}$ at different temperatures are then the slopes of the plots of the fractional weight loss under isothermal conditions versus $t^{0.5}$ as shown in Figures 9 and 10. These figures show that the weight loss reached the equilibrium value after a period of heating of about

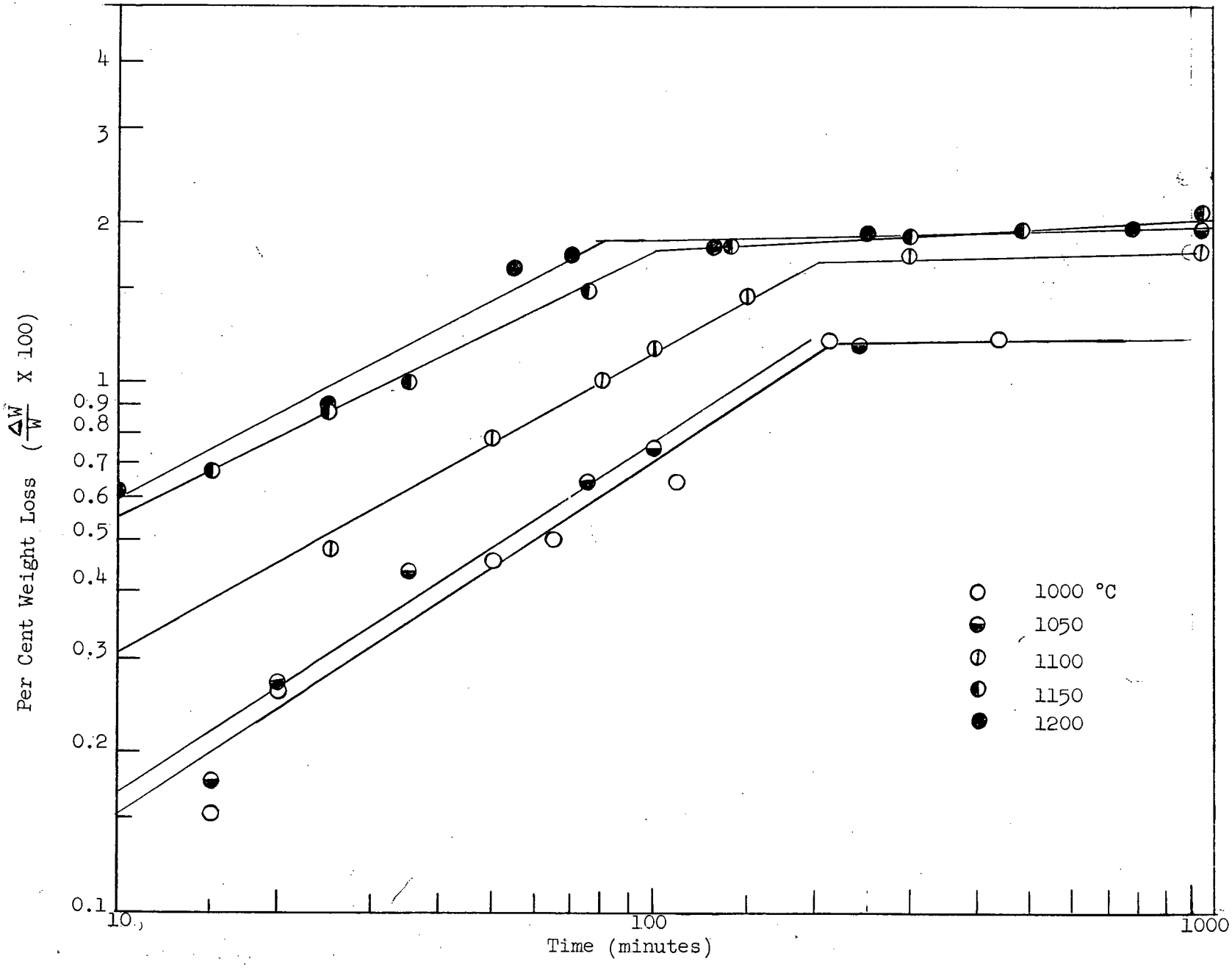

Figure 7. Per Cent Weight Loss as a Function of Time for $TiO_{1.92}$

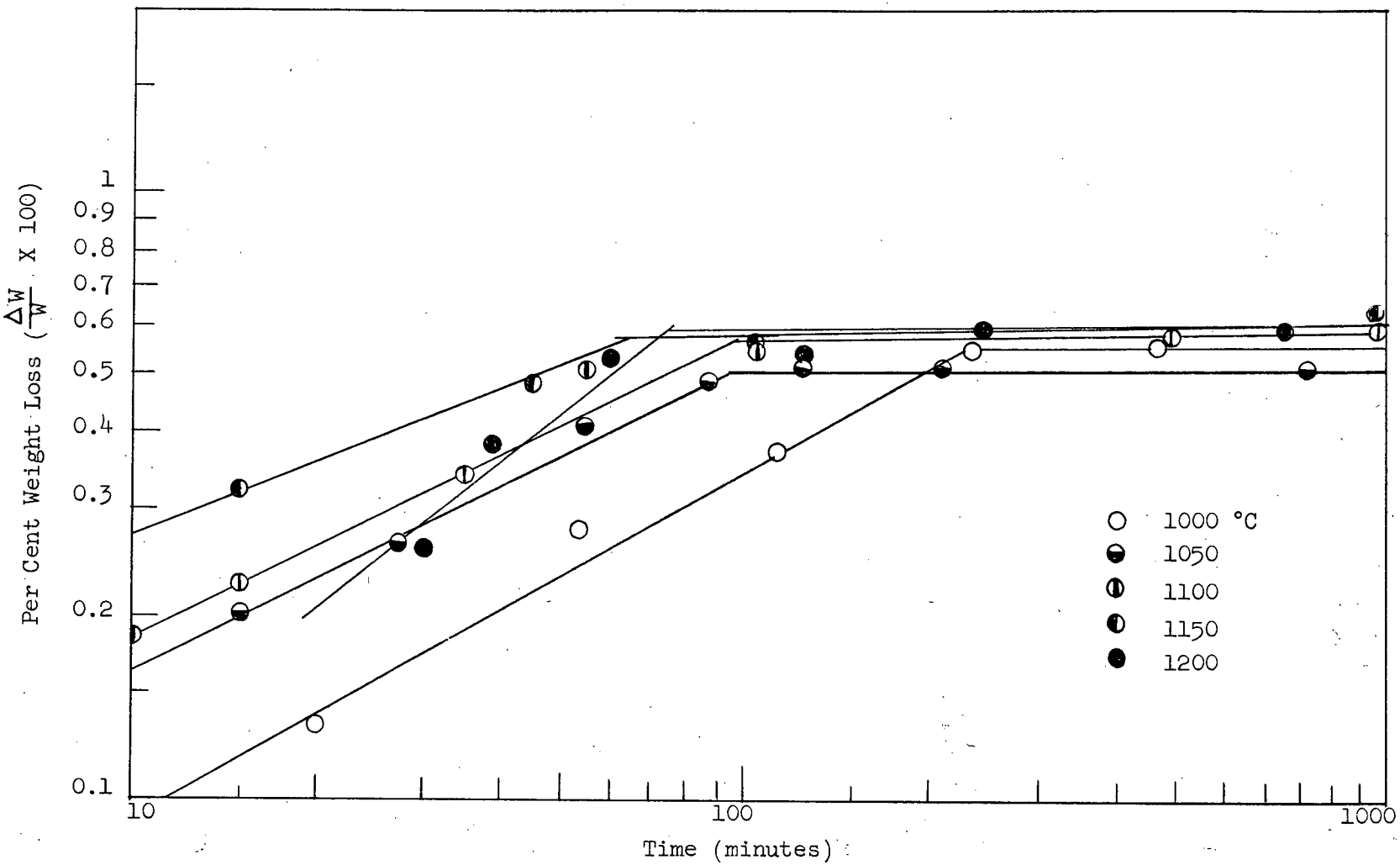

Figure 8. Per Cent Weight Loss as a Function of Time for $TiO_{1.98}$

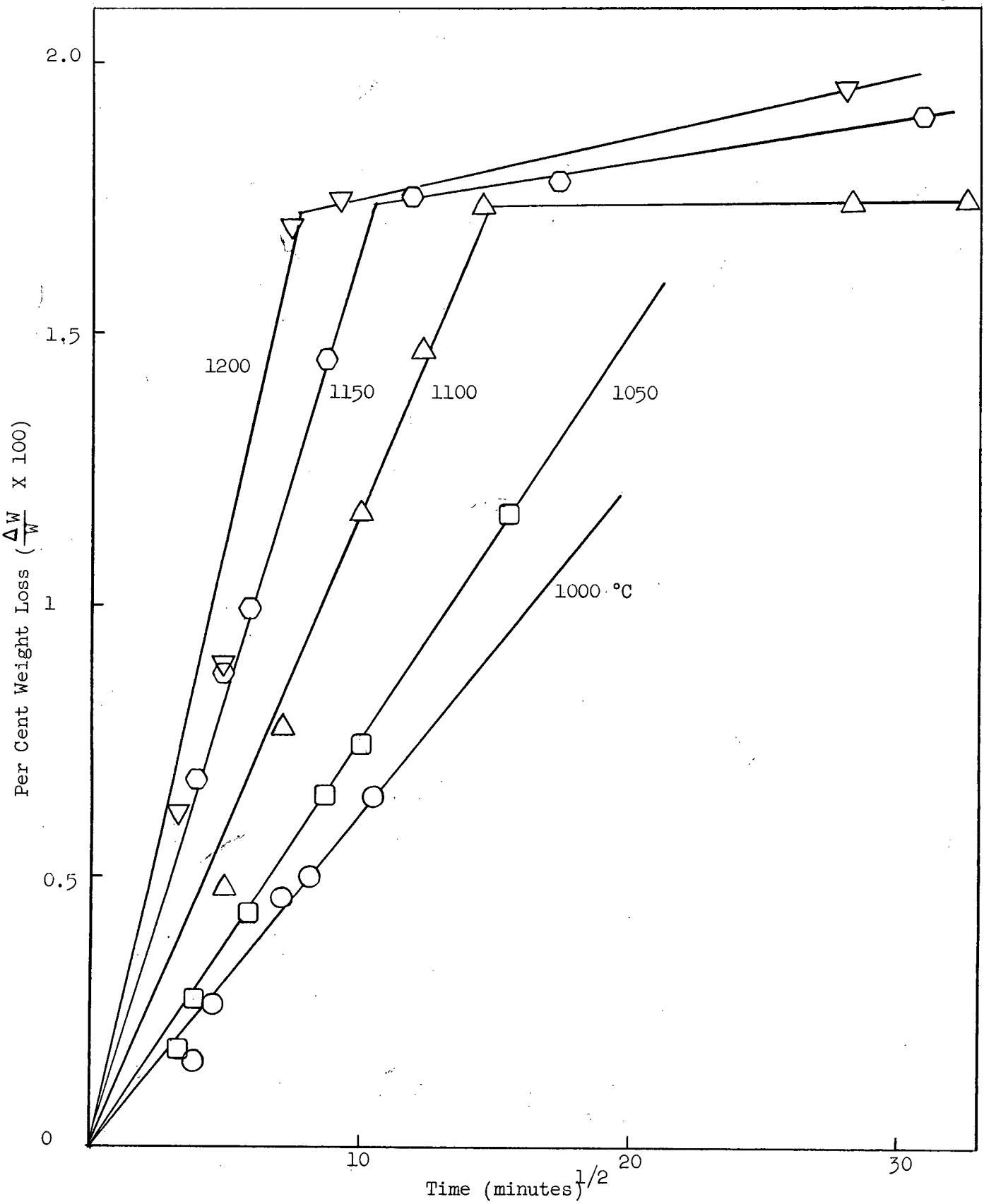

Figure 9. Per Cent Weight Loss Versus Square Root of Time for $TiO_{1.92}$

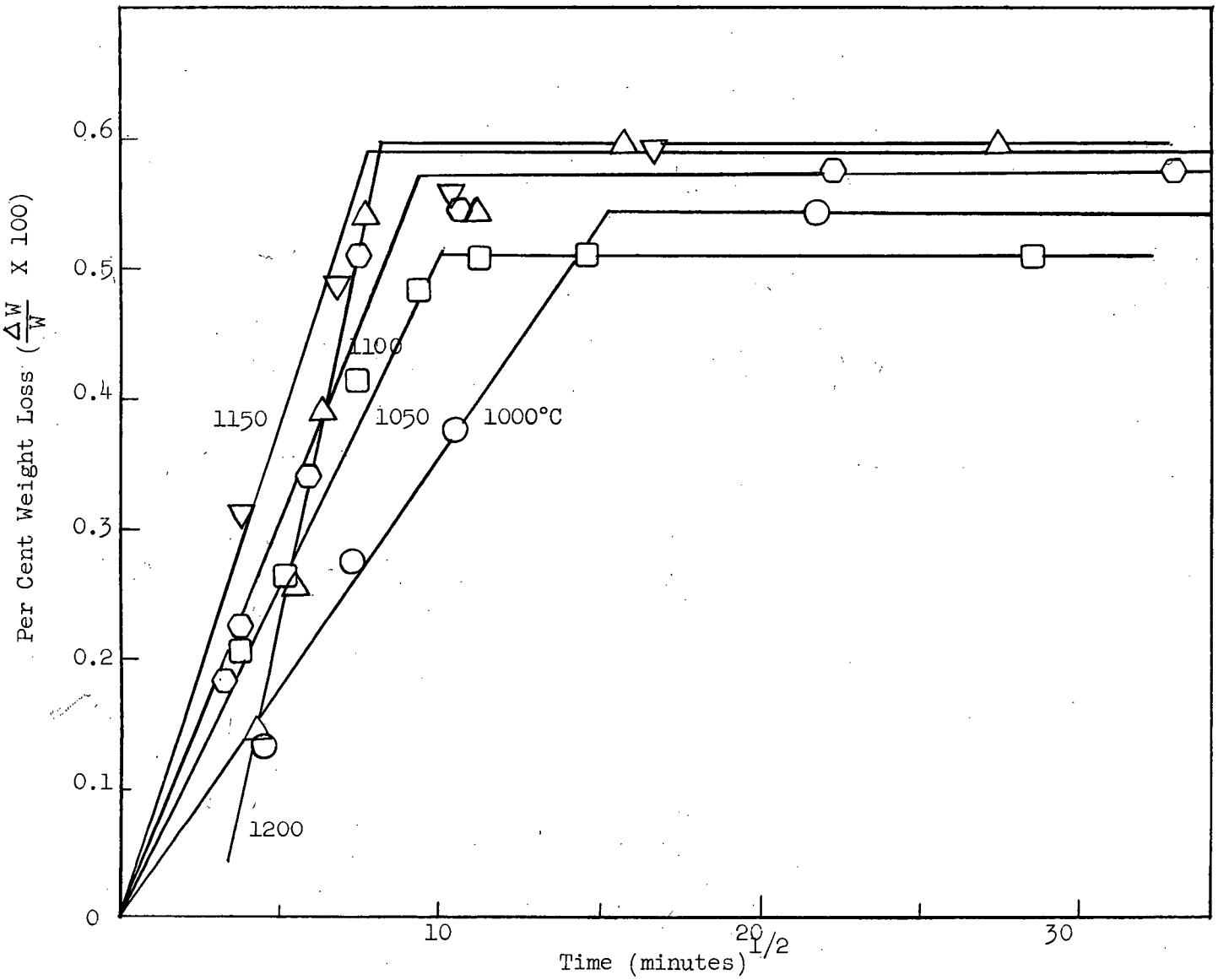

Figure 10. Per Cent Weight Loss Versus Square Root of Time for $TiO_{1.98}$

100 to 300 minutes. For this reason, only the data before 150 minutes of reduction were taken into account for the calculation of the slopes by the least squares method. The results are tabulated in Appendix I, Tables 1 and 2.

In order to determine the oxygen partial pressure dependence of the function A, it was assumed that the relationship took the form

$$A = K' \, PO_2^{\,x} \qquad .....(9)$$

$$\text{or} \quad A^{0.5} = K'^{0.5} \, PO_2^{\frac{x}{2}} \qquad .....(10)$$

where K' includes the specific reaction rate constant and any other variables affecting the rate. In logarithmic form, the relationship (10) will be

$$\log A^{0.5} = \frac{1}{2} \log K' + \frac{x}{2} \log PO_2 \qquad .....(11)$$

The experimental values of $\log A^{0.5}$ (Appendix I, Tables 1 and 2) have been plotted against $\log PO_2$ (Appendix III, Table 3) for each temperature and are shown in Figure 11. Although these curves are determined by two points only, the four plots can be considered as parallel within experimental error. The values of x obtained from the slopes of these plots are tabulated in Appendix I (Table 4) and give a mean value of $-\frac{1}{3}$.

On this basis, K' can be derived from the experimental value of $A^{0.5}$ using equation (11). The calculated values of K' are shown in Appendix I, Tables 1 and 2.

Provided the only temperature dependent term in K' is the rate constant, the slope of an Arrhenius plot will correspond to the activation energy for the rate determining step. These are shown in Figure 12 for both series of experiments.

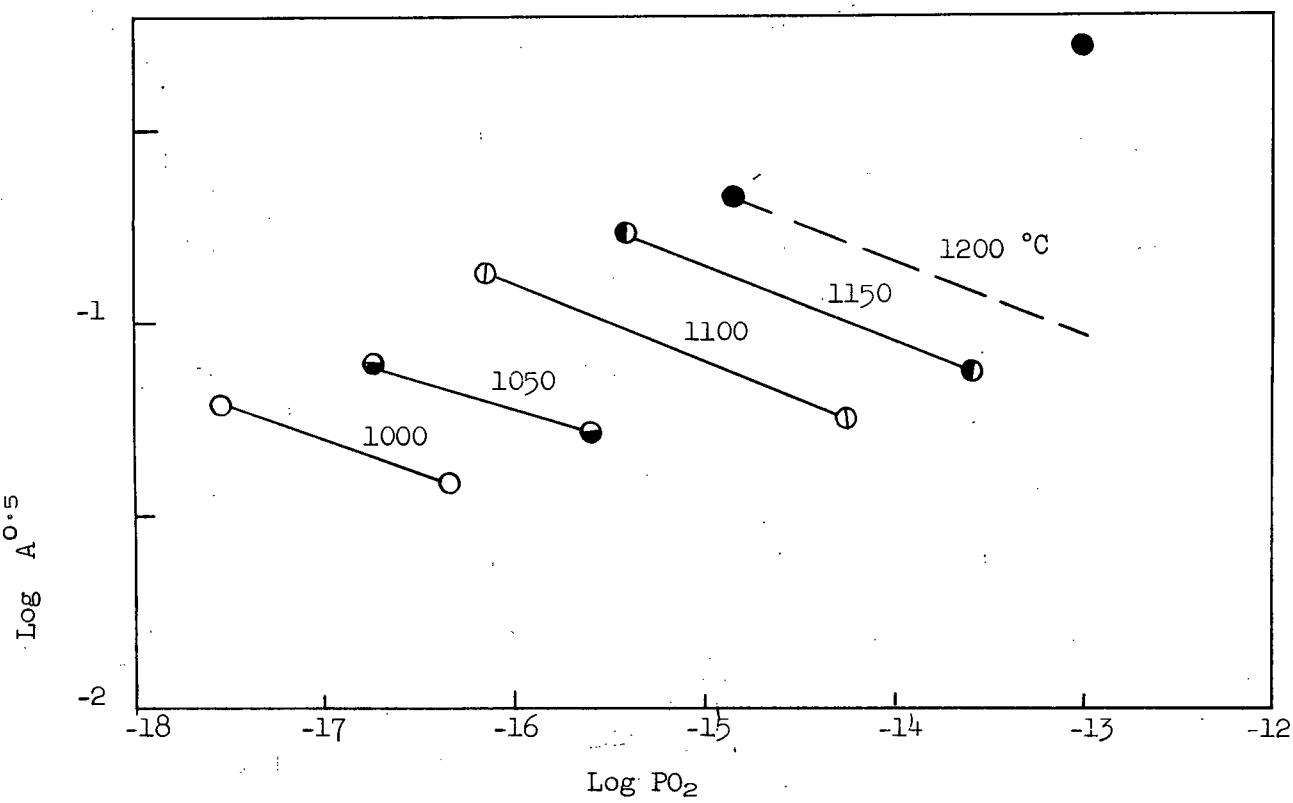

Figure 11. A Log-Log Plot for $A^{0.5}$ as a Function of Oxygen Partial Pressures at Different Temperatures

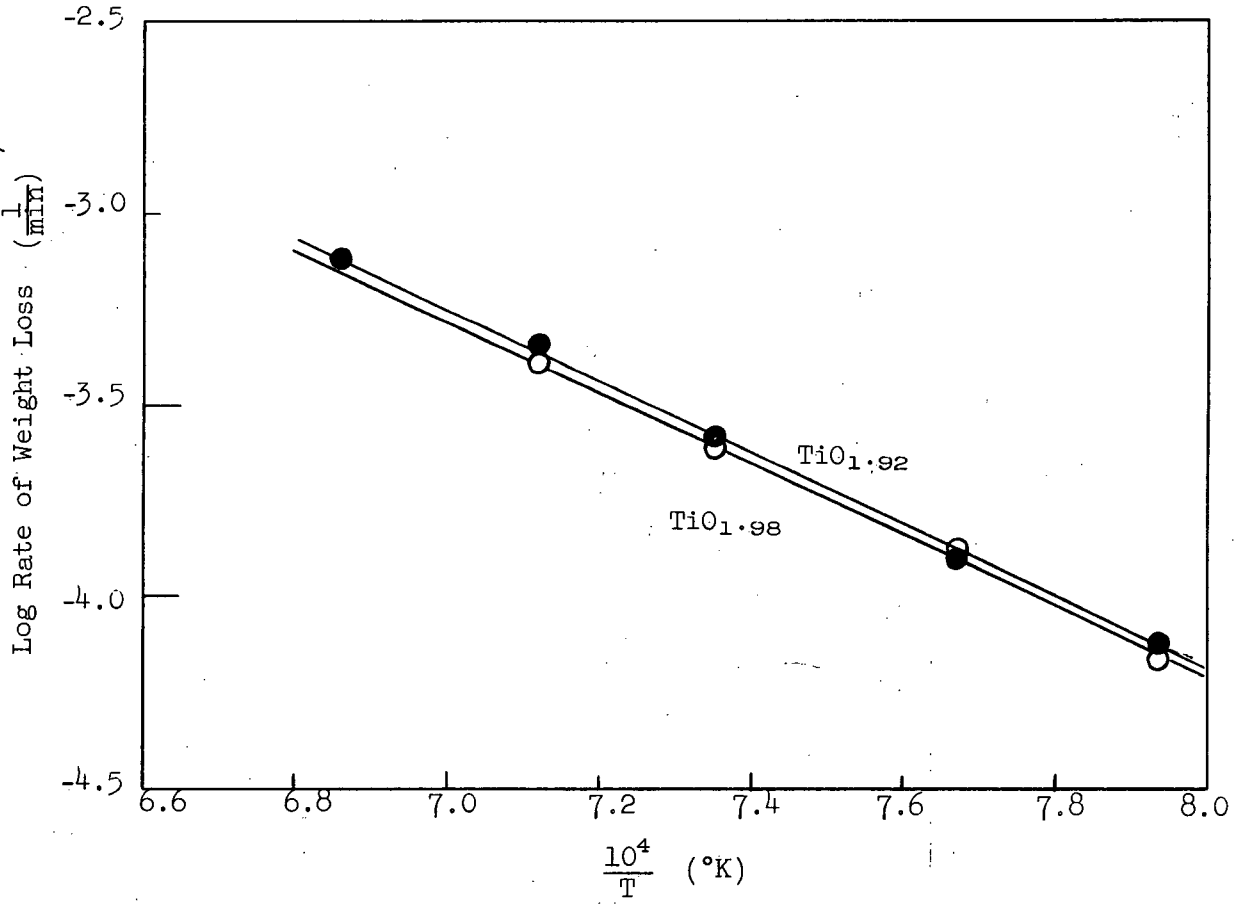

Figure 12. Temperature Dependence of Weight Loss

The corresponding value of the activation energy calculated from the slope is 82 ± 2 kcal/mole for both of these equilibrium compositions.

Grain Growth Study

The variation of the grain size as a function of the heating time was studied under controlled H_2/H_2O atmosphere over the temperature range of 1000°C to 1300°C. The photomicrographs as shown in Figure 13a, b, c, d, reveal the different stages of grain growth during the sintering process. These are very similar to those shown in Figure 3 (after Coble[5]). The exaggerated grain growth was expected to occur at or above the Sauerwald temperature T_S which for TiO_2 (m.p. 1900°C) lies between 1250 and 1425°C. Exaggerated grain growth was actually observed at 1250°C after 4000 minutes and at 1300°C after 1200 minutes of sintering as shown in Figure 13d.

Theoretical justification for results obtained in isothermal grain growth experiments was made initially by Beck et al.[25] and by Turnbull[26]. The average grain diameter correlated with time according to Turnbull is given as

$$D^2 - D_o^2 = K_1 \gamma V t \qquad .....(12)$$

where D is the average grain diameter at time t, D_o is the average original diameter at t = 0, K_1 is a rate constant and V is the atomic volume. Burke[27], however, deduced the following expression for grain growth on the assumption that the motivating force for grain-boundary migration during grain growth is the surface tension of the boundary, and that the radius of curvature of the boundary is proportional to the grain diameter

$$D^2 - D_o^2 = K_o t^n \exp\left(-\frac{Q}{RT}\right) \qquad .....(13)$$

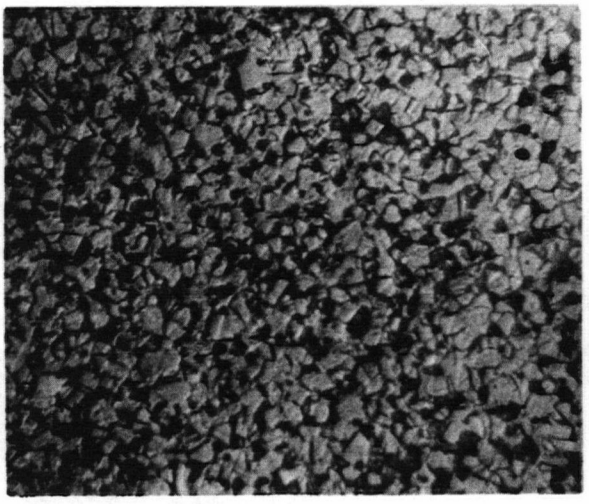

(a)
X 1500

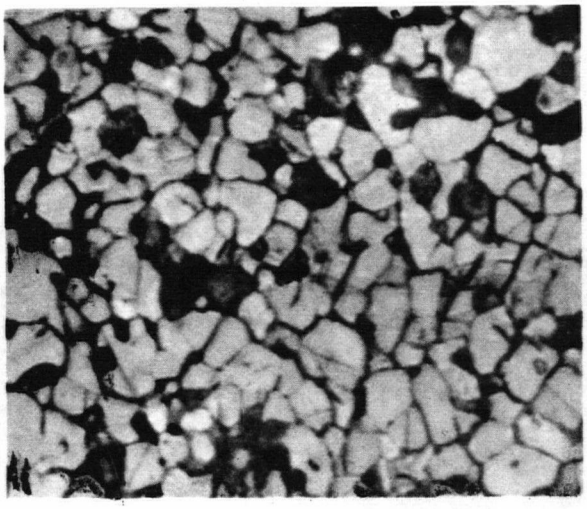

(b)
X 1500

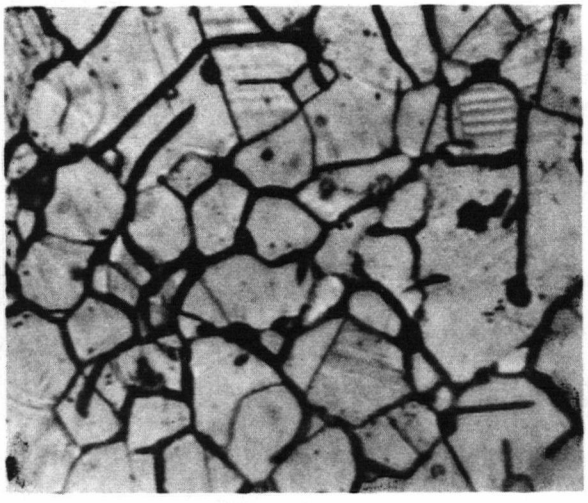

(c)
X 1500

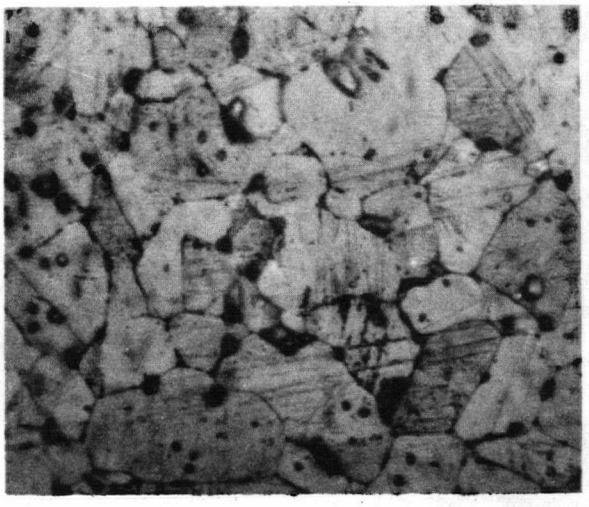

(d)
X 600

Figure 13. Typical Microstructures of Sintered $TiO_{1.92}$.

(a) Initial Stage - fired at 1150°C for 190 minutes,
(b) Intermediate Stage Showing Channel and Spherical Pores - fired at 1150°C for 280 minutes,
(c) Final Stage - fired at 1200°C for 2800 minutes,
(d) Beginning of Discontinuous Grain Growth - fired at 1300°C for 1200 minutes.

where K_o = a rate constant
n = the time exponent with a theoretical value of unity
Q = the activation energy for grain growth
R = gas constant
T = absolute temperature.

The grain size data which are tabulated in Appendix II were examined by plotting the log of the diameter of the grains versus log time in Figure 14. From the measurements of the slopes of these lines, it is apparent that the slopes do not equal the theoretical value of 1/2. Therefore, a plot of log $(D^2 - D_o^2)$ versus log t was done in Figure 15, the slopes of which indicate an average value of 0.6 ± 0.1 for n. In order to derive the value of the activation energy for grain growth, a final plot of $D^2 - D_o^2$ versus $t^{0.6}$ for each temperature was made, (Figure 16), the slope of which was the value of the rate constant, K, which varies with the absolute temperature (T) as, $K = K_o \exp\left(-\frac{Q}{RT}\right)$. The activation energy Q was then calculated from the slope of the Arrhenius plot (Figure 17), where log K was plotted against $\frac{1}{T}$. The derived value for the activation energy was 78 kcal/mole.

Sintering Study

Experiments were carried out to study the densification of rutile powder compacts in the temperature range of 1000 to 1300°C in air and in a reducing atmosphere. The reducing atmosphere was used in the sintering study as to obtain the equilibrium compositions for non-stoichiometric rutile of $TiO_{1.92}$ and $TiO_{1.98}$. The same atmosphere had also been used previously for weight loss and grain growth measurements.

The densification data are given in Appendix III, Table 1, for the final composition of $TiO_{1.92}$. A detailed study of the microstructure

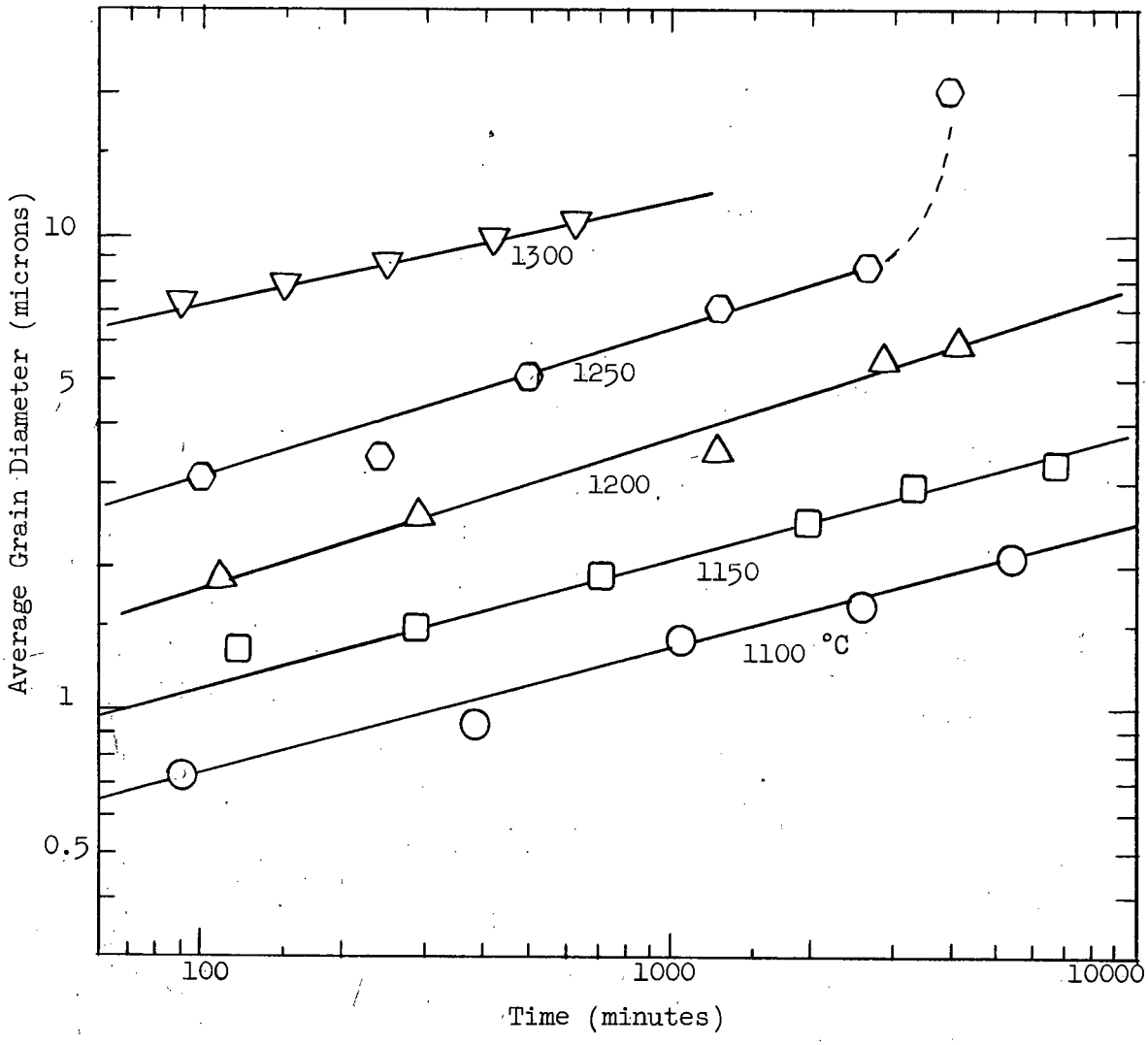

Figure 14. Log-Log Plot of Average Grain Diameter Versus Time

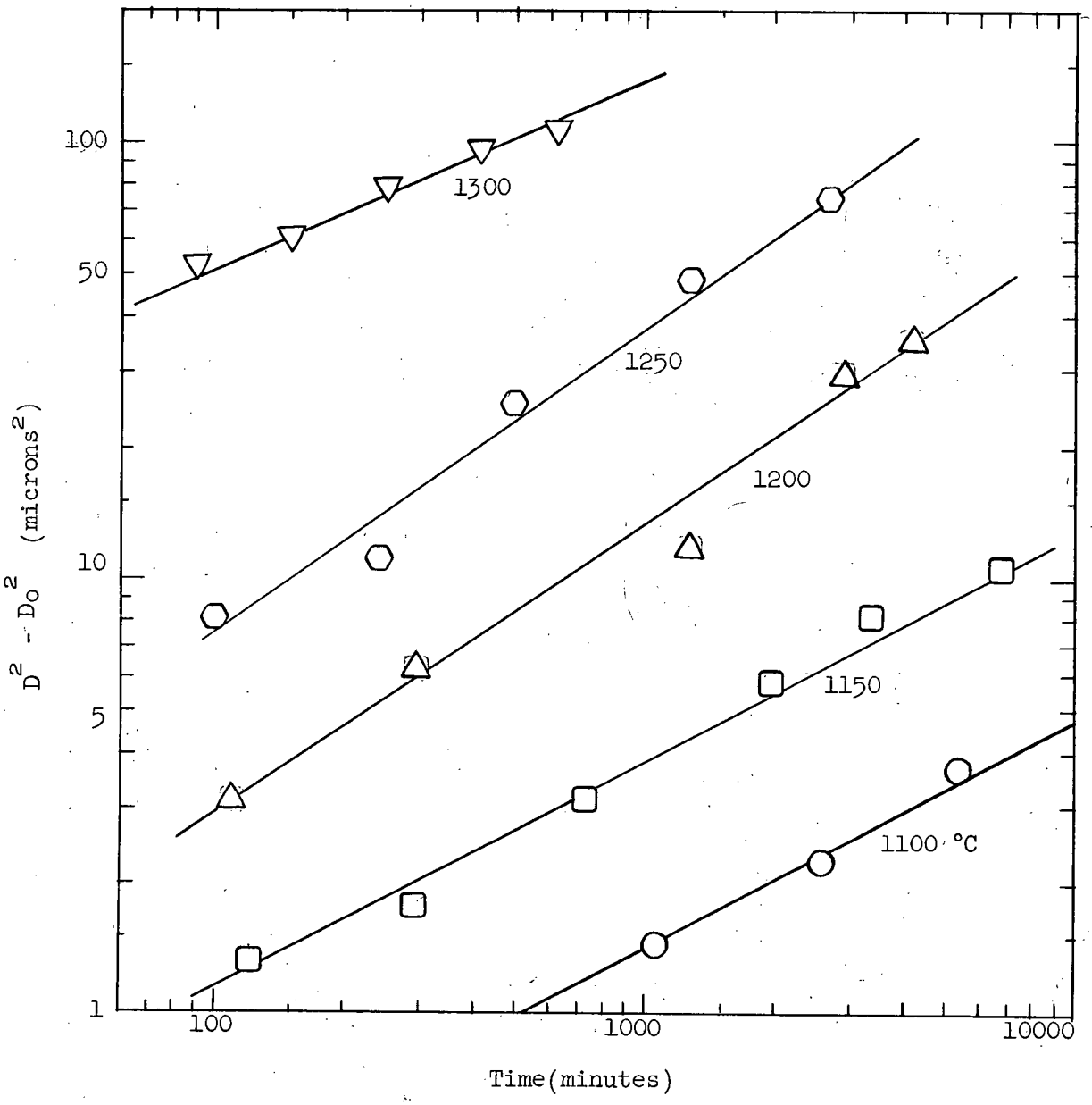

Figure 15. Grain Growth in $TiO_{1.92}$ Compacts with Temperature

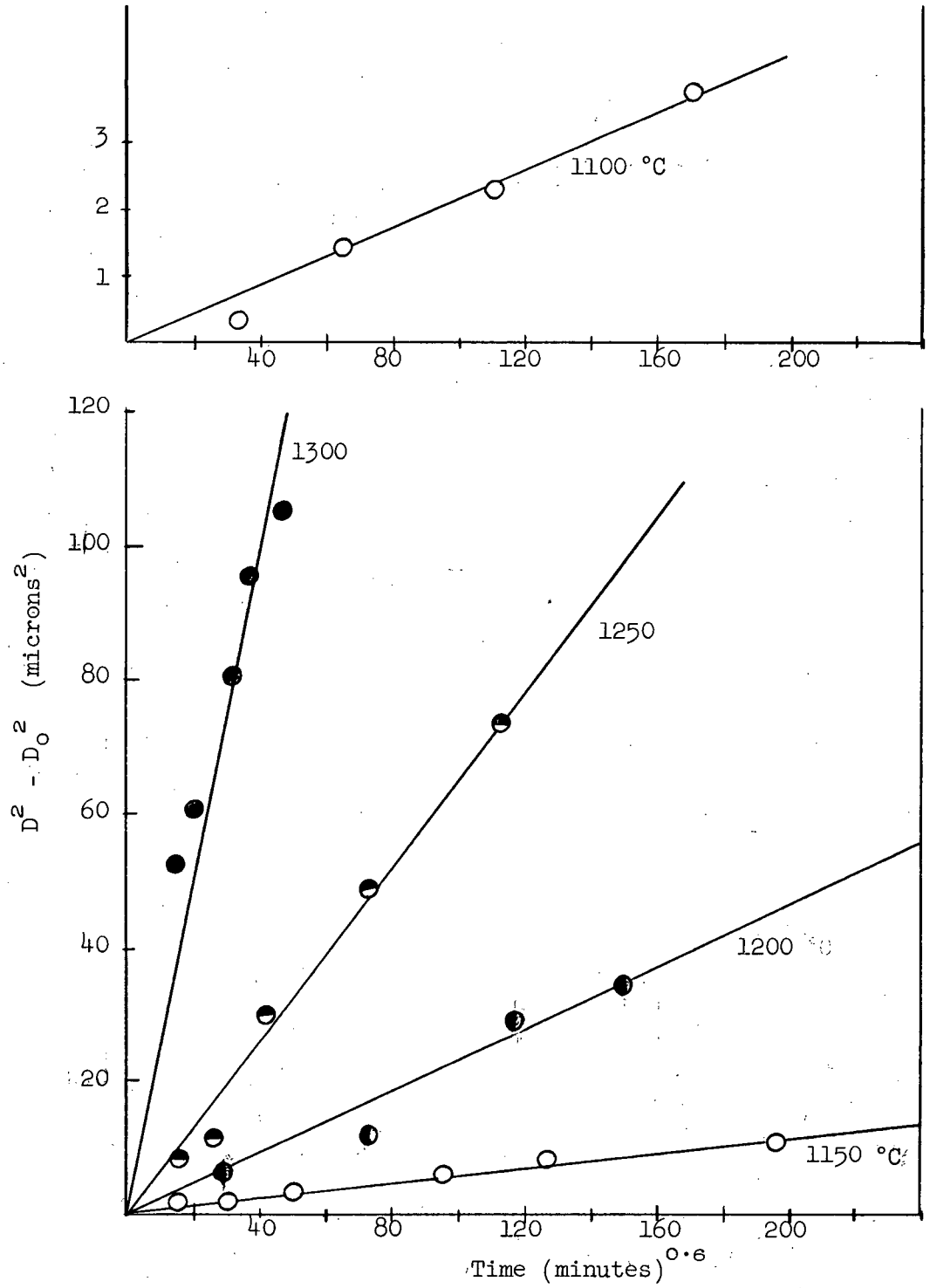

Figure 16. Isothermal Grain Growth

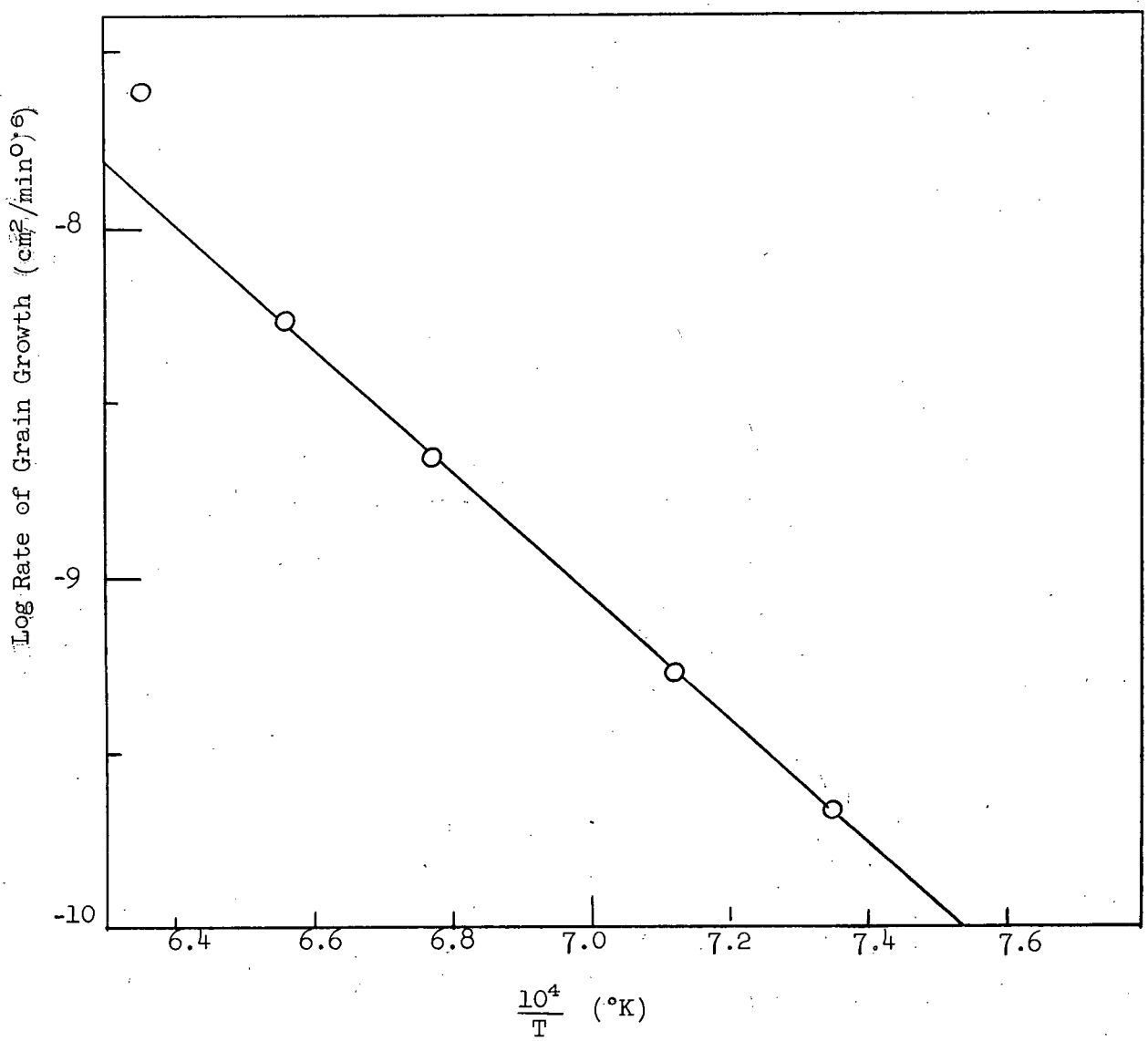

Figure 17. Logarithm of Grain Growth Rate Versus Reciprocal Temperature

as already shown in Figure 13a-d, revealed that the pores were in the form of channels, which partially filled up in the last stage. The pores became almost spherical in shape and were present in three- or four-grain corners, as was the case with the model proposed by Coble[5].

The isothermal densification (or shrinkage) data were converted to the relative density of the compact which was plotted against log time. The following equation derived by Coble[5]

$$\frac{dP}{dt} = \frac{N D_V \gamma a_o^3}{l^3 k T} \qquad \ldots\ldots(6)$$

yields on integration

$$P \Big]_{P_o}^{0} = - \frac{N D_V \gamma a_o^3}{A k T} \ln t \Big]_{t_o}^{t_f} \qquad \ldots\ldots(14)$$

where P_o is the porosity at time t_o and zero porosity at time t_f and assuming $l^3 = A\,t$, where l is the grain diameter at time t. The results are shown in Figure 18a, b, c, d, e, for the final composition of $TiO_{1.92}$. Similar investigation on the densification of $TiO_{1.98}$ and TiO_2 was carried out, but no detailed study was made on their grain growth. The results are shown in Figure A.III-1a, b, c, d, e, for $TiO_{1.98}$ and in Figure A.III-2 for TiO_2. The data are tabulated in Appendix III, Table 2. The variation of the composition of non-stoichiometric rutile as calculated from the weight loss measurements was also included in Figure 18 and Figure A.III-1 for the final compositions of $TiO_{1.92}$ and $TiO_{1.98}$ respectively.

From all these figures, it is quite apparent that the densification behaviour was completely changed after a certain time of heating. The densification was stopped in most cases, reaching an end-point density,

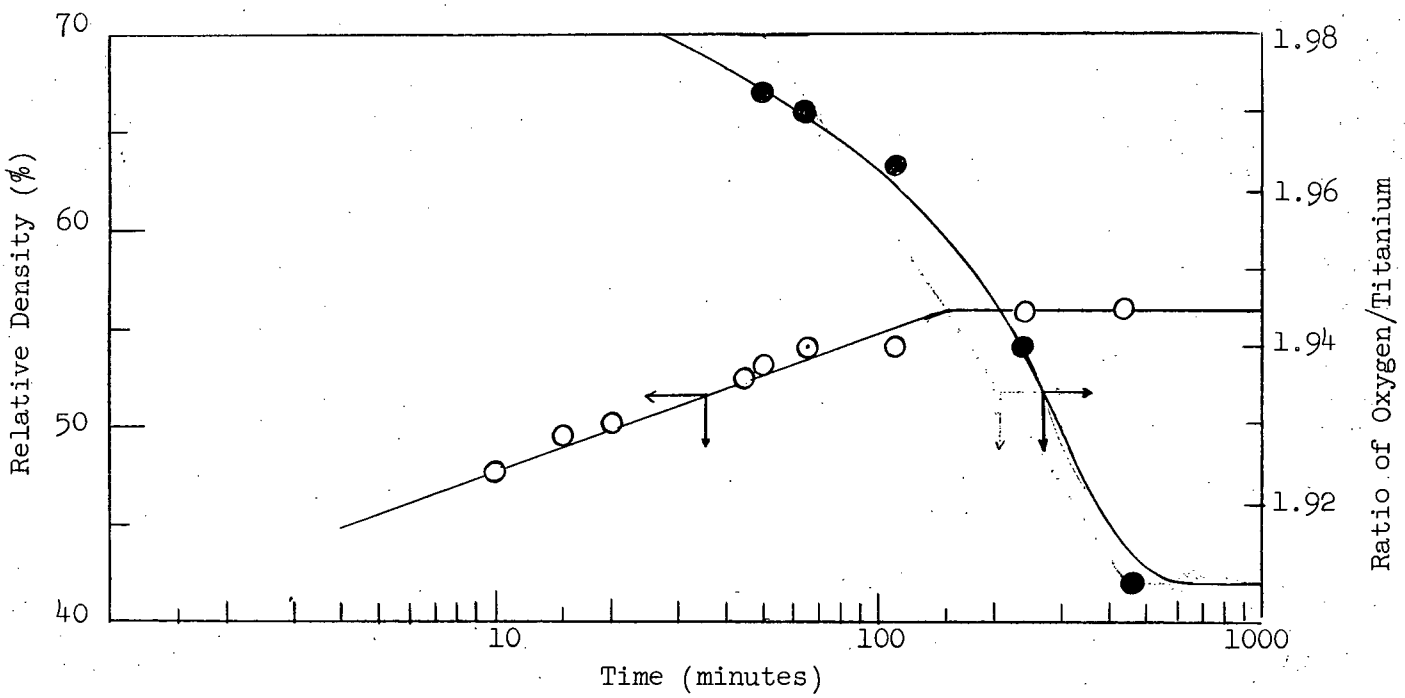

Figure 18a. Densification of Compacts for the Final Composition of $TiO_{1.92}$ at T = 1000°C.

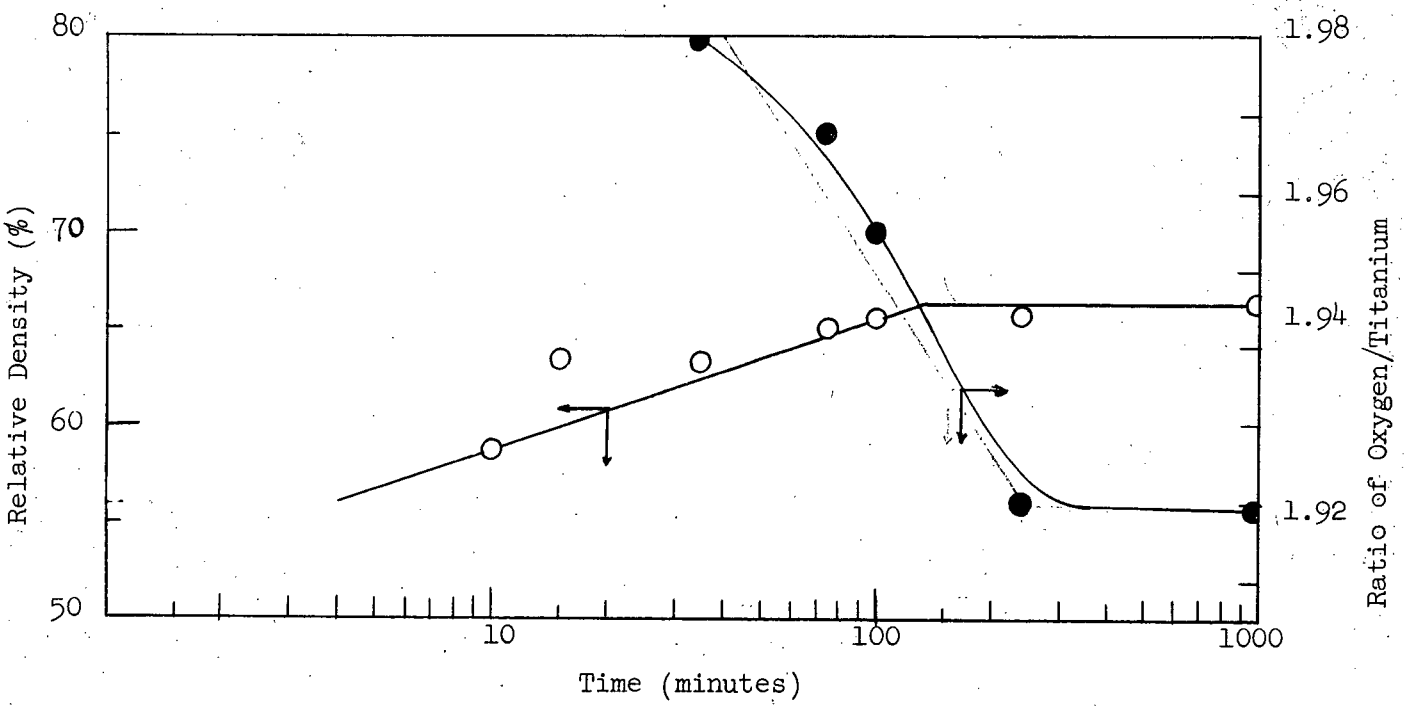

Figure 18b. Densification of Compacts for the Final Composition of $TiO_{1.92}$ at T = 1050°C.

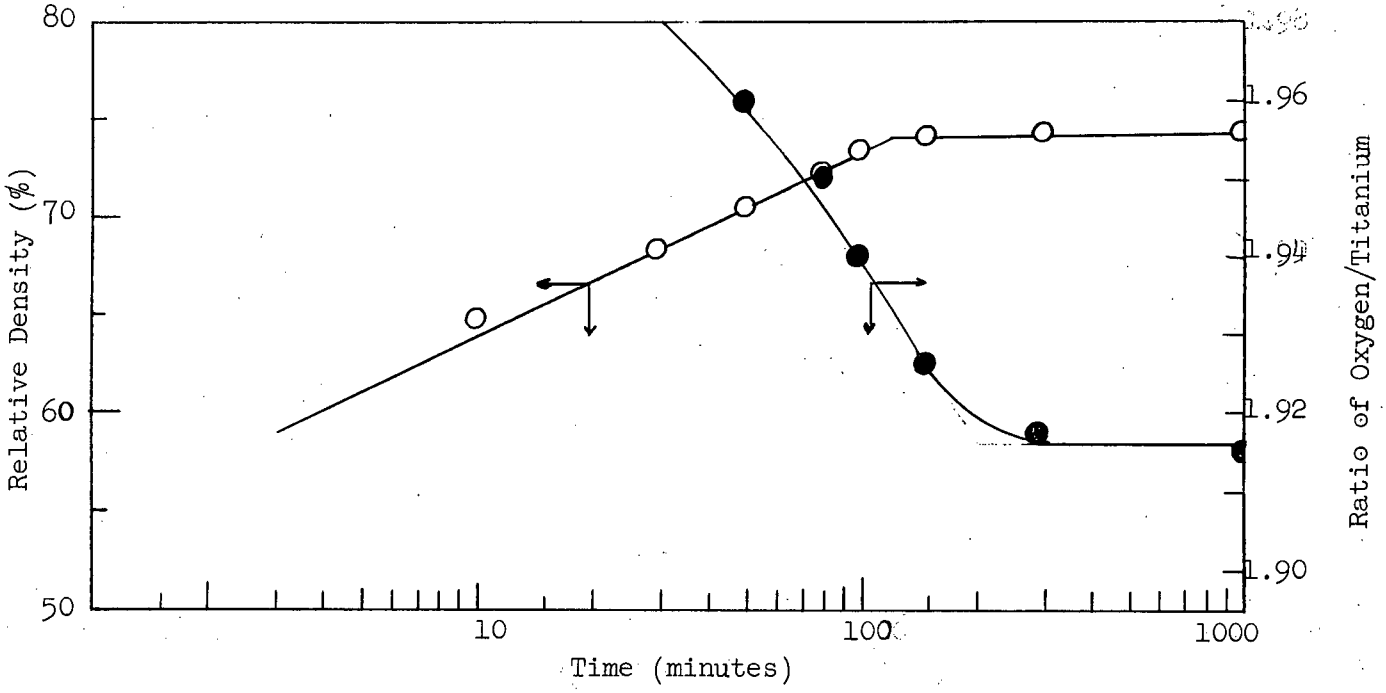

Figure 18c. Densification of Compacts for the Final Composition of $TiO_{1.92}$ at T = 1100°C.

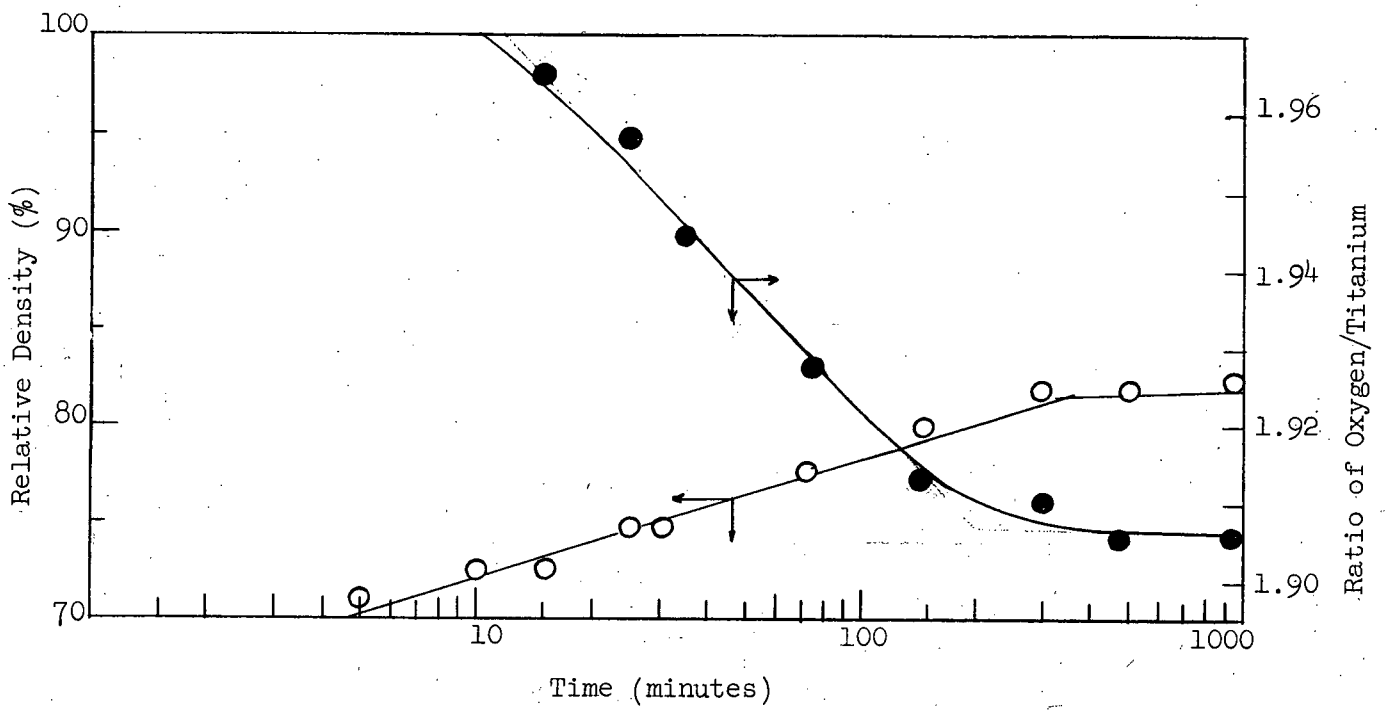

Figure 18d. Densification of Compacts for the Final Composition of $TiO_{1.92}$ at T = 1150°C.

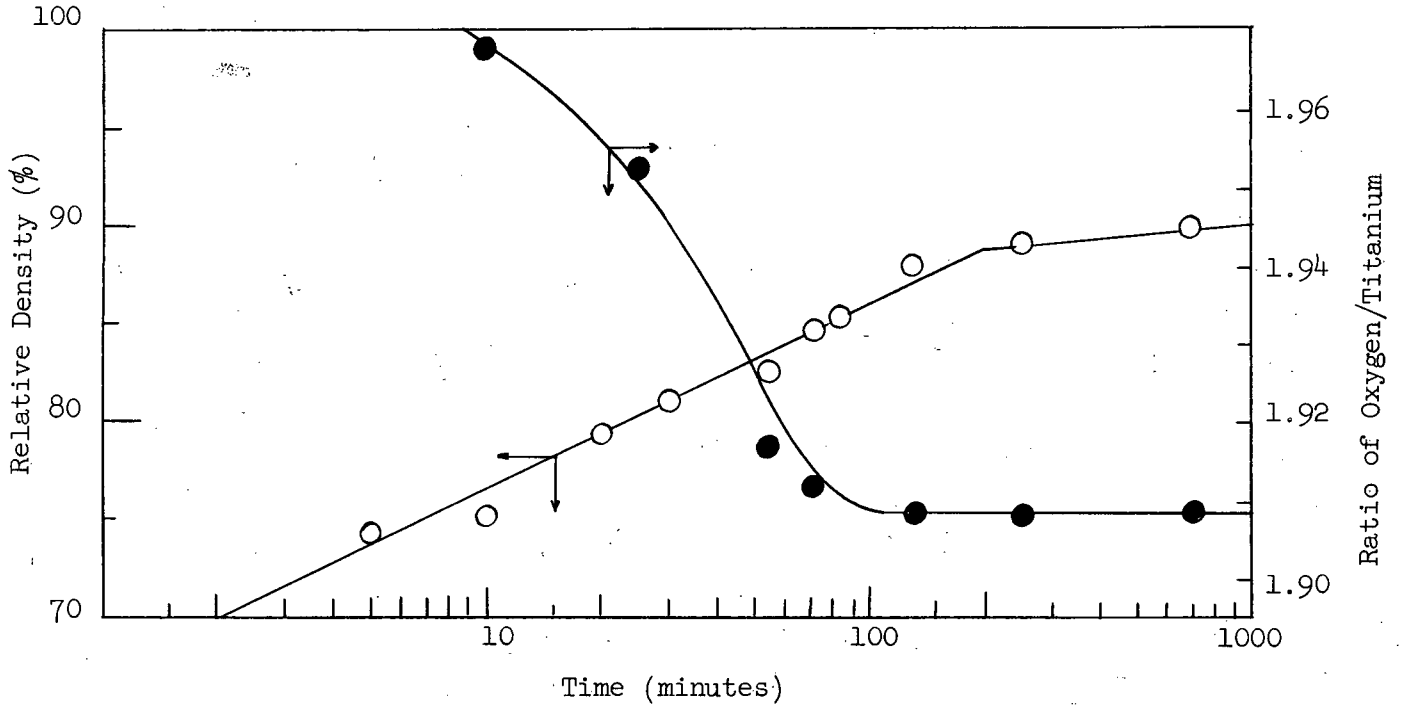

Figure 18e. Densification of Compacts for the Final Composition of $TiO_{1.92}$ at T = 1200°C

approximately at the same time as the equilibrium composition was reached for non-stoichiometric rutile. The end-point density monotonically increased with the increase of temperature of sintering. The break in the isothermal densification curves occurred after a heating time of 100 to 200 minutes for non-stoichiometric rutile and between 10 to 15 minutes for TiO_2.

In order to calculate the diffusion coefficients D_v in equation (14) it is only necessary to know the value of A experimentally as the value of the other constants are known. While investigating the isothermal grain growth of an equilibrium composition of $TiO_{1.92}$, it was found that the following expression satisfied the experimental data.

$$D^2 - D_o^2 = K\, t^{0.6} \qquad .....(15)$$

This equation is almost equivalent to

$$l^3 = D^3 = A\, t \qquad .....(16)$$

neglecting D_o^3, as the initial grain size D_o was very small, and A in equation (16) is equal to $K^{3/2}$.

Therefore, the plot of D^3 versus time was made for all temperatures, as shown in Figure A.III-3 (in Appendix III), the slopes of which give the values of A. The results are recorded in Appendix III, Table 3.

The slopes of the plot of the relative density versus log time at any temperature T are equal to

$$\frac{2.3\, N D_v \gamma a_o^3}{A k T}$$

Using N = 10, γ = 1000 ergs/cm^2, $a_o^3 = 1.57 \times 10^{-23}$cm^3, $k = 1.38 \times 10^{-16}$ ergs/deg. and the value of A (from Figure A.III-3) at different temperatures,

the corresponding diffusion coefficients (D_v) were calculated. The results are given in Table 4, Appendix III. An Arrhenius plot (Figure 19) of log D_v versus $(\frac{1}{T})$ produced an activation energy of 118 kcal/mole for diffusion.

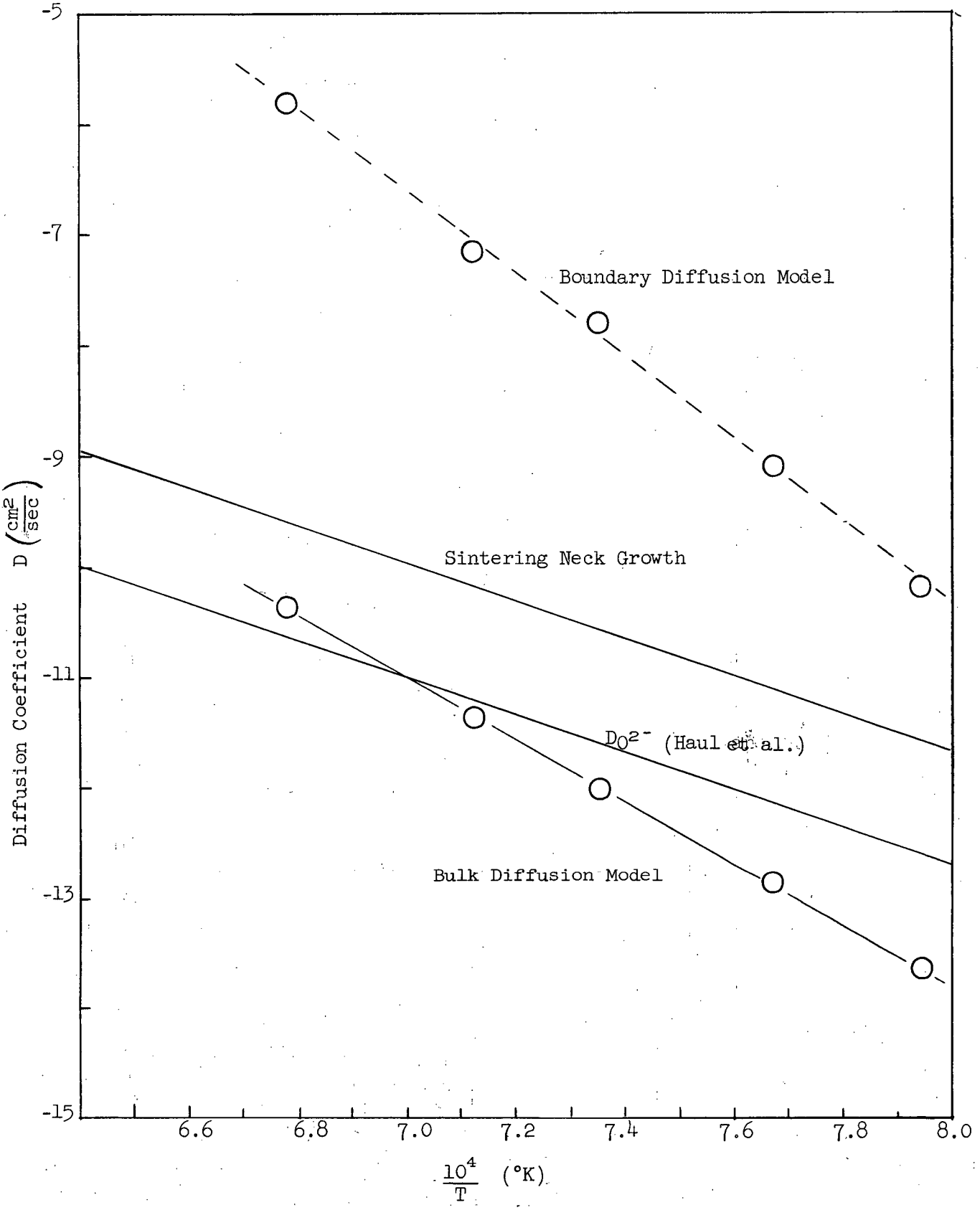

Figure 19. Diffusion Coefficient Versus the Reciprocal of the Absolute Temperature. Directly measured oxygen diffusion coefficients in single crystals are compared with values calculated from sintering experiments and models.

DISCUSSION

Defect Structures of Rutile

The reduction equation involving the creation of the oxygen ion vacancy and its two trapped electrons may be derived by using a model similar to that already advanced by Greener, Whitmore and Fine[28] for Nb_2O_5 and Whitmore and Kawai[11] for TiO_2. This equation is

$$O_1^{2-} \rightleftharpoons \frac{1}{2} O_{2(g)} + V_{O}^{2-} + 2\,\theta \qquad \text{.....(17)}$$

where O_1^{2-} is an oxygen ion in a normal lattice position and V_O^{2-} is an oxygen ion vacancy in which the two electrons were trapped in the form of two Ti^{+++} ions.

The law of mass action was applied to equation (17) with the result

$$K = P_{O_2}^{1/2} [V_O^{2-}] [\theta]^2 \qquad \text{.....(18)}$$

as the concentration of trapped electrons is twice the concentration of oxygen vacancies

$$[\theta] = 2 [V_O^{2-}]$$

The equation (18) becomes in terms of the oxygen vacancy concentration

$$[V_O^{2-}] = \left(\frac{K}{4}\right)^{1/3} P_{O_2}^{-1/6} \qquad \text{.....(19)}$$

This equation shows that under equilibrium conditions the concentration of vacancies is proportional to the -1/6 power of the oxygen partial pressure. Equation (19) can be rewritten as

$$[V_O^{2-}] = 0.63\, P_{O_2}^{-1/6} \exp\left[-\frac{\Delta H°f}{3RT} + \frac{\Delta S°f}{R3} \right] \qquad \text{.....(20)}$$

where $\Delta H°f$ and $\Delta S°f$ are the enthalpy and entropy of formation for reaction (17). After removing the temperature independent term from the

experimental function, equation (20) becomes

$$[V_{O^{2-}}] = C P_{O_2}^{-1/6} \left(\frac{\Delta H°f}{3\,RT}\right) \qquad .....(21)$$

where C stands for $(0.63 \exp\frac{\Delta S°f}{R3})$.

Weight Loss Study

Buessem and Butler[29] derived a similar expression to interpret the total weight loss of rutile on equilibration with various oxygen atmospheres. Their equation was

$$2\,Ti^{4+} + O^{2-} \rightleftharpoons V_{O^{2-}} + \frac{1}{2}\,O_2 + 2Ti^{3+} \qquad .....(22)$$

of which the equation constant is

$$K_{(T)} = C \exp\left[\frac{H_{AV} + 2H_{Ti^{3+}} + \frac{1}{2}\,H°_{O_2}}{k\,T}\right]$$

where H_{AV}, $H_{Ti^{3+}}$ and $H°_{O_2}$ are the enthalpy of the anion vacancy of Ti^{3+} and of oxygen gas in the standard state.

From the experimental data, Buessem and Butler obtained an enthalpy value of 83 ± 10 kcal/mole. By using a value of -53.75 kcal/mole (for the change of standard state) they obtained for

$$H_{AV} + 2H_{Ti^{3+}} = 136.65 \pm 10 \text{ kcal/mole.}$$

Interpreting Cronemeyer's data on conductivity of rutile[30] in this manner revealed that

$$H_{AV} + 2Ti^{3+} = 127.05 \text{ kcal/mole.}$$

A comparison of equation (21) and these data shows that

$$\Delta Hf = 127.05 \text{ (or } 136.65 \text{ kcal/mole)}$$

or $\frac{\Delta Hf}{3} = 42.35$ kcal/mole for the defect reaction represented by equation (21).

In the present case, no attempt was made to determine the detailed mechanism of reduction of TiO_2 since this did not fall within the scope of this investigation. However, the activation energy of 82 ± 2 kcal/mole obtained is identical to the enthalpy of reaction (22) obtained by Buessen and Butler[29]. This would suggest that the rate-determining step may be the formation of an oxygen-ion vacancy.

Grain Growth

The predicted increase of grain size in a normal grain size distribution with no inhibiting second phase has been observed to follow the square root of time. However, impurities in the lattice or nonuniformity in the grain size distribution and shape in the original material can cause the grain growth to be a function of a smaller power of time. This can be expressed as

$$D^2 - D_o^2 = K t^n \qquad 0 < n \leqslant 1 \qquad .....(15)$$

with n = 1 in the theoretical case. Another explanation for lower than theoretical values for n has been advanced by Burke[27]. In many grain growth investigations, the original material contains a disproportionately large number of fine grains. Therefore the average radius of curvature of the grain boundary will increase more rapidly than predicted by the theoretical equation where n has the value of 1.

In this study most of the measurements plotted in Figures 7 and 8 relate to continuous cylindrical pores interconnected at the grain boundaries. The second stage of pore shrinkage, i.e. the isolated pore phase, was observed only at the higher temperatures and after long periods of heating. This is illustrated by Figure 13d, of a specimen heated at 1300°C for 1200 minutes.

But this change in pore shape does not influence the relation (15) which is the same as long as exaggerated grain growth does not occur. Therefore, particular attention was given at the higher temperatures used, 1250 and 1300°C to avoid the measurements influenced by exaggerated grain growth.

The results of the present investigation for $TiO_{1.92 \pm 0.01}$ can be represented by the following expression

$$D^2 - D_o^2 = K_o\, t^{0.6} \exp\left(-\frac{78,000}{RT}\right)$$

The time exponent n has the value of 0.6 instead of the theoretical value n = 1. For the non-stoichiometric composition of $TiO_{1.98 \pm 0.01}$, n = 0.6 while for TiO_2 n = 1, (Appendix III, Table 5)

The variation of the value of the exponent n with the change of stoichiometry of the compound has also been evaluated for UO_2[31,32]. The value of n changed from n = 1.2 to n = 0.8 for UO_2 to UO_{2+x}. Table II compares the value of n for different ceramic oxides as determined from the grain growth data.

Table II.

Values of Exponent n for Different Ceramic Oxides

Oxide	n	Reference
UO_{2+x}	0.8/0.9	31
UO_2	1.2	32
CaO	1.0	33
MgO	1.0	33
Al_2O_3	0.66 (0.62-0.74)	12
$Ca_{0.15}\, Zr_{0.85}\, O_{1.85}$	0.8	34
Present Work TiO_2	0.60	-

Temperature Dependence of Grain Growth

Before discussing the significance of the present value of the activation energy for the grain growth of TiO_{2-x} it is informative to consider the activation energies for the grain growth process in other ceramic oxides. For the purpose of comparison, the energies for the self diffusion of the components in such systems are also included in Table III.

Table III.

Activation Energy Data for Different Ceramic Oxides

Oxides	Activation Energy for grain growth	(Ref.)	Activation Energy for self diffusion of the cation	(Ref.)	Activation Energy for self diffusion of the anion	(Ref.)
Al_2O_3	153	(12)	114	(35)	152	(36)
MgO	60	(33)	79	(37)	62.4	(38)
$Ca_{0.15}Zr_{0.85}O_{1.85}$	80	(34)	109 for $Ca^{2+}Zr^{4+}$	(39)	29.8	(40)
UO_2	87	(32)	88	(41)	60	(41)
TiO_2	78	-	-	-	74	(43)

As is evident, the activation energy for grain growth of oxides corresponds to the energy required for the diffusional process of either one of the two components. On this basis, it is always considered that the grain growth of oxides is controlled by a diffusion mechanism.

In the present investigation, the activation energy obtained for the grain growth study is 78 kcal/mole for $TiO_{1.92} \pm 0.01$. The temperature behaviour of the oxygen self-diffusion coefficient has been determined by Haul and Just[42] using Linde rutile single crystals and O^{18} isotopic exchange technique. Their diffusion data can be represented as follows

$$D_{O^{2-}} = 1.6 \exp\left(-\frac{74,000}{RT}\right) \frac{cm^2}{sec}$$

between the temperature range 850 to 1300°C.

An expression for the intrinsic oxygen self-diffusion coefficient for non-stoichiometric rutile, $D_{O^{2-}}$ has been derived in Appendix IV, the final form of which is

$$D_{O^{2-}} = D_o \exp -\left(\frac{\Delta H°f}{3\,RT} + \frac{U}{RT}\right)$$

where D_o is the usual frequency factor, $\Delta H°f$ is the energy to form an oxygen vacancy, and U is the activation energy for oxygen vacancy migration.

By comparing the experimental value with the thermodynamic calculation

$$\frac{\Delta H°f}{3} + U = 74 \text{ kcal/mole}$$

and by taking $\Delta H°f = 127.05$ kcal/mole from Cronemeyer's data, the energy for vacancy migration U is about

$$74 - \frac{127}{3} = 31.6 \text{ kcal/mole}$$

Similar calculations with the present grain growth data produced a value of 35 kcal/mole for the activation energy for migration of the oxygen vacancy. These results are in good agreement and it appears reasonable enough to suggest that oxygen ion diffusion is the likely rate-controlling step in the process of grain growth of non-stoichiometric titania.

Sintering

The microstructures as shown in Figure 13a-d, reveal the different stages of densification. They are almost similar to those depicted by Coble (Figure 3). The intermediate stage is shown in Figures 13a and b, which are photomicrographs of specimens heated at 1150°C for 190 minutes and 280 minutes respectively. In Figure 13b, the pores are at the junction of three —grain corners, indicating the presence of continuous pores. The final stage begins when the pore phase is eventually pinched off. The presence of some pores at the four-grain corners in Figure 13c, indicates that the specimen had reached the final stage of sintering. The microstructures of specimens sintered at higher temperatures revealed both trapped pores in the grains and pores at the grain boundary corners as shown in Figure 13d. Existence of trapped pores in the grains in all specimens, which were fired at or above 1250°C suggests that some degree of discontinuous grain growth occurred in all cases. This is also evident from the density-time curves (Figure 18a-e), where in every case an end-point density was observed.

Exaggerated grain growth was carefully avoided in this investigation by carrying out all experiments below 1300°C ($\approx$ Sauerwald temperature in the case of TiO_2). A comparison of Figures 13b and 13d shows that the uniformity in grain and pore size which was present at the beginning of the sintering process later disappeared. At the later stage several grains grew larger at the expense of smaller ones. On further heating, shrinkage of the pores in the grain boundaries was observed, which resulted in some increase in relative density of the compacts.

Annealing twins were observed in the specimens after 2000 minutes of sintering at or above 1250°C; no study was made to test the effect of this on the grain growth or sintering.

Density-Time Curve

Isothermal density-time curves in Figure 18a-e, present the effect of temperature only, as the effects of atmospheres were not determined, although the oxygen partial pressure in the system was varied at different temperatures. The compacting pressure was found to have a significant effect on the initial relative density and on the densification rate and so was kept constant. The initial relative density of all specimens was 1.96 gm/cm^3, particularly for the non-stoichiometric equilibrium composition of $TiO_{1.92}$. The use of compacts of such low bulk density eliminated to some extent the presence of the density gradient produced by die wall friction, although this could not be completely avoided. Large shrinkage rate anisotropy was not observed.

The initial part of density-time curves never extended to the final stage of sintering according to Figure 13, so that the change of slope cannot be attributed to the change of pore shape. In addition, according to Coble[12], the change of pore phase continuity should occur at about 95% of the theoretical density of the compact, which, in this investigation, was never achieved in any specimen. The change of slope in all cases occurred when the composition of the non-stoichiometric rutile under the reducing atmosphere reached an equilibrium value. Thus, it appears that the change of rate is not a function of change of pore shape but is related to the formation of oxygen vacancies in the system during the pre-equilibrium stage.

O'Bryan and Parravano[10] measured the rate of neck growth between rutile spheres in an atmosphere of H_2/H_2O (= 10) and observed similar breaks in their isothermal neck growth rate curves. They explained this observation on the basis of polygonization of monocrystalline rutile spheres and assumed that the specimens reached equilibrium almost immediately during heating.

The significance of the slopes of the density versus log time curves is not known. The slope may be affected by the initial particle size, particle shape and also by inhomogeneities in initial bulk density, pore size distribution, and particle alignment. The problem, then, is to determine whether the diffusion model is supported by the linearity of the curves.

Diffusion Coefficient

The linear region of the density-time curve in the pre-equilibrium stage of densification was used to calculate the diffusion coefficient. The observed increase in densification rate with increasing temperature is typical of thermally-activated processes in ceramics. Each curve has roughly the same character. The slopes vary, but cannot be interpreted quantitatively, and therefore the change in slope from one line to another is not understood.

The apparent diffusion coefficients calculated from the results are shown in Figure 19 where they were plotted as log D against 1/T. Other data plotted in this figure are Haul and Just's[42] directly measured diffusion coefficients for oxygen (determined by isotopic exchange technique) and Whitmore's[11] apparent diffusion coefficients calculated for measurements of neck growth between two spheres.

The diffusion coefficients calculated from intermediate stage measurements are lower than those from neck growth measurements by an order of magnitude but agrees with the directly measured diffusion coefficients. Only order-of-magnitude reliability may be attached to the individual models or results, and therefore the discrepancy does not disprove the model applied in this case. However, the calculated activation energy of 118 kcal/mole in the present case is not in agreement with other results. This is reflected

in the difference of slopes of the lines as shown in Figure 19. This discrepancy may be attributed to some of the factors involved in the calculation of the diffusion coefficients. The error in the measurement of grain size would affect the factor A (equation (16)). Similarly, the error in the measurement of the shrinkage values would affect the slope of the density-time curve. The cumulative effect of these two on the calculated diffusion coefficients may be considerable. This is particularly true for the specimens sintered below 1100°C. The changes in the grain size and in the dimensions of the specimens with time below 1100°C were very small. Any error in the measurement of these two parameters would have a large effect on the value of diffusion coefficients at lower temperatures.

The effect of the initial shape of the grain on the shrinkage rate is not known. Coble's[5] original model was based completely on the spherical grains. In the present case, the initial grains are like flakes. These are expected to change into a minimum surface area configuration in the earliest stage of sintering, as these flakes have large surface energy associated with them. The steps involved in this change of configuration are not known and, therefore, its effect on the overall shrinkage rate cannot be evaluated.

The effect of oxygen partial pressures on the diffusion coefficients was evaluated by the following procedure. The isothermal grain growth rates of the equilibrium compositions of $TiO_{1.98}$ and TiO_2 at 1200°C were determined. The data were plotted as D^3 (where D = average grain diameter) versus time. The slope of the lines produced the values of A for these two compositions.

Using the shrinkage data at 1200°C the diffusion coefficients for the equilibrium compositions of $TiO_{1.98}$ and TiO_2 were calculated. The results are tabulated in Appendix III in Tables 5 and 6. In the following table the diffusion coefficients and their respective oxygen partial pressures are compared. It can be seen that the diffusion coefficients were not significantly affected by the change of oxygen partial pressure in the system.

Table IV

Calculated Diffusion Coefficients at Different Oxygen Partial Pressures

Composition	Diffusion Coefficient (D_V) at 1200°C cm^2/sec	Oxygen Partial Pressure in Atmosphere
$TiO_{1.92}$	4.32×10^{-11}	1.41×10^{-15}
$TiO_{1.98}$	5.84×10^{-11}	1×10^{-13}
TiO_2	12.51×10^{-11}	0.21

In view of the disagreement between the value of the activation energy obtained in this investigation and that found in other sintering studies, attempts have been made to apply other available models for densification. Two other models are currently available. Coble[5] in addition to his bulk diffusion model, proposed a grain boundary diffusion model on the understanding that densification might proceed by the migration of the grain boundary. Coble derived the following equation for the grain boundary diffusion

$$P = \left[2 \frac{D_b W \delta a_o^3}{1^4 k T} t \right]^{2/3} \qquad .....(23)$$

where P = volume fraction pores at time t
D_b = diffusion coefficient of atoms in the grain boundary
W = grain boundary width, and other factors similar to similar to equation (6).

The values of boundary diffusion coefficient D_b were calculated using equation (23) and the porosity data of the equilibrium composition of $TiO_{1.92}$. The results and calculations are given in Appendix V. These are plotted in Figure 19 to compare with the other results. According to this figure, the bulk diffusion model gives a better fit for the present result.

Johnson and Cutler[13] very recently derived an equation to interpret their linear shrinkage data of alumina compacts. The equation has the following form

$$\frac{\Delta L}{L_o} = \left(\frac{K \gamma a_o^3 D}{k T r^p} \right)^m t^m \qquad \ldots\ldots(24)$$

where $\frac{\Delta L}{L_o}$ = fractional shrinkage
K = numerical constant
γ = surface energy
D = self diffusion coefficient
a_o^3 = vacancy volume
r = particle radius
t = time
m,p = constants

In this equation, the value of the time exponent m varies between 0.25 to 0.50 according to the geometry of the contact points, such as spherical, paraboloid or 160° cone on a plane etc. The fractional linear shrinkage data in the present investigation were also plotted against time in a log-log scale. The value of m is found to be less than 0.1 in this case. The significance of such a low value is not known and as a consequence no attempt was made to calculate the diffusion coefficient using this generalized equation.

CONCLUSIONS

The reduction of rutile was carried out to two final compositions of $TiO_{1.92}$ and $TiO_{1.98}$ using different H_2/H_2O atmospheres. The fractional weight loss with time was found to follow a parabolic relationship. An Arrhenius plot using rates which were corrected for oxygen partial pressure dependence produced an activation energy of 82 ± 2 kcal/mole. The weight loss measurements under equilibrium conditions carried out by other investigators produced an enthalpy of 83 ± 10 kcal/mole. This may suggest that the rate determining step is the oxygen ion vacancy formation.

Grain growth data for the equilibrium composition of $TiO_{1.92} \pm 0.01$ can be explained by the following expression

$$D^2 - D_o^2 = K_o \; t^{0.6} \; \exp\left(-\frac{78,000}{RT}\right)$$

The value of time exponent n was found to be different from the theoretical value of unity for $TiO_{1.92}$ and $TiO_{1.98}$. It was equal to one for the grain growth of stoichiometric rutile. The activation energy for oxygen ion diffusion in TiO_2 determined by oxygen isotopic exchange technique was found to be 74 kcal/mole. On this basis, it is justifiable to suggest that oxygen ion diffusion is the likely rate-controlling step for the grain growth of the $TiO_{1.92}$ non-stoichiometric composition.

Densification of the final equilibrium composition of $TiO_{1.92}$ was explained using a sintering model proposed by Coble. The values of the diffusion coefficient calculated in this investigation were of the right order of magnitude but the activation energy for the diffusion process calculated from these data did not agree with that of other workers. This discrepancy is explained on the basis of errors in the measurements, inhomogeneities in the compact and other possible factors which affect the densification process.

RECOMMENDATIONS FOR FUTURE INVESTIGATIONS

This study on grain growth and sintering of rutile compacts under reducing atmospheres was the first attempt to apply a model of densification on rutile powder compacts.

The effect of initial compacting pressures on grain growth and densification should be carried out using rutile powders of known and simple geometry. Also keeping the particle shape as simple as possible, initial grain size effect on the densification rate should be investigated. This data by correlating with the grain growth measurements should help to identify the factors which control the value of the time exponent in the generalized expression of the grain growth. With the availability of a plasma, the powdered particle should be spheroidized before other experiments are undertaken. This should eliminate the heterogeneity in contact angles and in number of contacts per particle. An observation of the number of contacts per particle during densification, as well as the measurement of surface area of the compacts would perhaps explain the drop in rate of densification once the equilibrium non-stoichiometric composition has been reached in rutile. The influence of grain growth inhibiting elements should be investigated in order to reach the theoretical density in the compacts.

To isolate the effect of reduction on the densification rate, the powdered particles should be reduced to a non-stoichiometric equilibrium composition before the sintering study is carried out.

BIBLIOGRAPHY

1. G. C. Kuczynski, "Powder Metallurgy", p. 11, Ed., W. Leszynski, Interscience Publishers Inc., New York and London, (1961)

2. W. J. Moore, "Physical Chemistry", p. 504, Prentice-Hall Inc., N.J., (1955).

3. W. D. Kingery and M. Berg, J. Appl. Phys. 26, 1205 (1955).

4. G. C. Kuczynski, "Powder Metallurgy", p. 1-16, The Iron and Steel Institute and the Institute of Metals, London, (1963).

5. R. L. Coble, J. Appl. Phys. 32, 787 (1961).

6. W. D. Jones "Fundamental Principles of Powder Metallurgy", Edward Arnold Press, London (1960).

7. C. Zener, see C. S. Smith, Trans. A.I.M.E., 175, 15 (1948).

8. G. C. Kuczynski, "Kinetics of High Temperature Processes", p. 37, Ed., W. D. Kingery, Technology Press and John Wiley and Sons, (1958).

9. L. F. Norris and G. Parravano, J. Am. Ceram. Soc., 46, 449 (1963).

10. H. M. O'Bryan, Jr., and G. Parravano, "Powder Metallurgy", p. 191, Ed., W. Leszynski), Interscience Publishers Inc., New York and London, (1961).

11. D. H. Whitmore and Toshihiko Kawai, J. Am. Ceram. Soc., 45, 375 (1963).

12. R. L. Coble, J. Appl. Phys. 32, 793 (1961).

13. D. L. Johnson and I. B. Cutler, J. Am. Ceram. Soc. 46, 545 (1963).

14. P. W. Clark, J. H. Cannon and J. White, Trans. Brit. Ceram. Soc. 52, 1 (1953).

15. A. H. Webster and N. F. H. Bright, The Effects of Furnace Atmospheres on the Sintering Behaviour of Uranium Oxide, Mines Branch Research Report R2, Department of Mines and Technical Surveys, Ottawa, February 5, 1958.

16. R. W. G. Wyckoff, Crystal Structure Handbook, Interscience Publishers, New York (1948).

17. M. E. Straumanis, T. Ejima and W. J. James, Acta. Cryst. 14, 493 (1961).

18. E. A. Gulbransen and K. F. Andrew, J. Metals 1; Trans. A.I.M.E., 185, 741 (1949).

19. Willy Kinna and Willy Knorr, Z. Metallkunde, 47, 594 (1956).

20. M. H. Davies and C. E. Birchenall, J. Metals 3; Trans. A.I.M.E., 191 877 (1951).

21. Karl Hauffe, Reactionen in und an Festen Stoffen, II, p. 135, Springer-Verlag, Berlin (1955).

22. a) J. Stringer, Acta Met. 8, 758 (1960).
b) P. Kofstad, K. Hauffe and H. Kjollersdal, Acta. Chem. Scand. 12, 239 (1958).

23. Tentative Method for Determining the Average Grain Size of Metals, A.S.T.M. Designation E 112-55 T, A.S.T.M. Standards, Part 1, (1955) p. 1435.

24. W. H. McKewan, Trans. A.I.M.E., 224, 2 (1962).

25. P. A. Beck, J. C. Kremer, L. J. Demer, and M. L. Holzworth, Metals Technol. 14, (1947); Tech. Pub. No. 2280; Trans. A.I.M.E. 175 372 (1948).

26. David Turnbull, J. Metals 3; Trans. A.I.M.E., 191, 661 (1951).

27. J. E. Burke, Trans. A.I.M.E. 180, 73 (1949).

28. E. H. Greener, D. H. Whitmore and M. E. Fine, J. Chem. Phys. 34, 1017 (1961).

29. W. R. Buessem and S. R. Butler, "Kinetics of High Temperature Processes", Ed., W. D. Kingery, Technology Press and John Wiley and Sons, p. 13 New York, (1959).

30. D. C. Cronemeyer, Phys. Rev. 87, 876 (1952).

31. J. R. MacEwan and V. B. Lawson, J. Am. Ceram. Soc., 45, 42 (1962).

32. I. Amato, R. L. Colombo and A. M. Protti, J. Am. Ceram. Soc. 46, 407 (1963).

33. A. V. Daniels, Jr., R. C. Lowrie, Jr., Rn L. Gibby and Ivan B. Cutler, J. Am. Ceram. Soc. 45, 282 (1962).

34. T. Y. Tien and E. C. Subbarao, J. Am. Ceram. Soc., 46, 489 (1963).

35. A. E. Paladino and W. D. Kingery, J. Chem. Phys. 37, 957 (1962).

36. Y. Oishi and W. D. Kingery, J. Chem. Phys. 33, 480 (1960).

37. Roland Linder and G. D. Parfitt, J. Chem. Phys. 26, 182 (1957).

38. Y. Oishi and W. D. Kingery, J. Chem. Phys. 33, 905 (1960).

39. W. H. Rhodes and R. E. Carter, "Ionic Self-Diffusion in Calcia-Stabilized Zirconia" presented at the Sixty-Forth Annual Meeting, The American Ceramic Society, New York, April 30, 1962. Symposium on Kinetics of Ceramic Reactions No 1-25-63, Am. Ceram. Soc. Bull. 41, 283 (1961).

40. W. D. Kingery, J. Pappis, M. E. Doty and D. C. Hill, J. Am. Ceram. Soc., 42, 393 (1959).

41. J. Belle, A. B. Auskern, W. A. Bostrom and F. S. Susko, "Diffusion Kinetics of Uranium Dioxide", U.S. Atomic Energy Comm. Report No. WAPD-T-1155, (1960).

42. R. Haul, D. Just and G. Dümbgen, "Reactivity of Solids", p. 65, Ed., J. H. DeBoer, Elsevier Publishing Company, Amsterdam, (1961).

APPENDIX I.

Table 1.

Weight Loss Data for $TiO_{1.92} \pm 0.01$

Temperature of Furnace °C.	$\frac{\Delta W}{W} \times 100$ %	Time t min	$t^{0.5}$	$A^{0.5}$ ($\frac{i}{min}^{0.5}$)	log $A^{0.5}$	log P_{O_2}	-0.5 log P_{O_2}	-1/3 log $K^{0.5}$
1000	0.153	15	3.87	6.116	-1.214	-17.53	-2.92	-4.134
(7.94)	0.260	20	4.52	X 10^{-2}				
	0.461	50	7.045					
	0.500	65	8.06					
	0.648	110	10.53					
	1.211	210	14.51					
	1.250	430	20.50					
1050	0.173	10	3.165	7.4677	-1.1275	-16.765	-2.794	-3.9215
(7.67)	0.270	15	3.87	X 10^{-2}				
	0.430	35	5.90					
	0.646	75	8.66					
	0.740	100	10.00					
	1.170	240	15.50					
	1.970	1065	32.55					
1100	0.480	25	4.98	12.641	-0.898	-16.16	-2.693	-3.591
(7.35)	0.775	50	7.04	X 10^{-2}				
	1.170	100	10.00					
	1.465	150	12.22					
	1.730	300	14.50					
	1.745	1055	32.45					
1150	0.678	15	3.87	15.536	-0.781	-15.412	-2.568	-3.349
(7.12)	0.871	25	4.98	X 10^{-2}				
	0.990	35	5.90					
	1.450	75	8.66					
	1.750	140	11.82					
	1.775	300	17.30					
	1.900	470	31.05					
	1.900	1065	32.55					
1200	0.613	10	31.65	22.327	-0.651	-14.85	-2.475	-3.126
(6.86)	0.890	25	4.98	X 10^{-2}				
	1.693	55	7.40					
	1.740	70	9.23					
	1.750	130	11.42					
	1.800	250	15.85					
	1.972	780	28.00					

Table 2.

Weight Loss Data for $TiO_{1.98 \pm 0.01}$

Temperature of Furnace °C.	$\frac{\Delta W}{W} \times 100$ %	Time t min	$t^{0.5}$	$A^{0.5}$ $\frac{1}{(min)^{0.5}}$	log $A^{0.5}$	log P_{O_2}	-0.5 log P_{O_2}	-1/6 log $K^{0.5}$
1000	0.132	20	4.47	3.7428	-1.4265	-16.376	-2.729	-4.2194
(7.94)	0.276	53	7.28	X 10^{-2}				
	0.376	113	10.62					
	0.540	233	15.28					
	0.542	473	21.76					
	0.542	1443	38.00					
1050	0.203	15	3.87	5.155	-1.288	-15.60	-2.60	-3.888
(7.67)	0.265	27.5	5.23	X 10^{-2}				
	0.415	55	7.42					
	0.486	87	9.33					
	0.510	125	11.18					
	0.510	215	14.65					
	0.510	810	28.45					
1100	0.186	10	3.165	5.667	-1.2474	-14.236	-2.373	-3.6204
(7.35)	0.225	15	3.87	X 10^{-2}				
	0.340	35	5.90					
	0.510	55	7.42					
	0.545	105	10.26					
	0.573	490	22.18					
	0.573	1075	32.80					
1150	0.310	15	3.87	7.3358	-1.135	-13.59	-2.265	-3.400
(7.12)	0.487	45	6.72	X 10^{-2}				
	0.555	105	10.26					
	0.590	275	16.58					
	0.645	2555	50.65					
	0.645	4440	66.70					
1200	0.140	24	4.13	5.170	-0.287	-13.00	-2.170	-2.457
(6.86)	0.255	30	5.47	X 10^{-1}				
	0.380	38	6.16					
	0.534	60	7.75					
	0.534	125	11.18					
	0.598	245	15.65					

Table 3.

Oxygen Partial Pressures

Temperature of Furnace °C.	Temperature of the Bubbler °C.	P_{H_2O} mm of Hg	$\frac{P_{H_2}}{P_{H_2O}}$	log P_{O_2}
A. For $TiO_{1.92} \pm 0.01$				
1000	23	21.068	35.2	-17.53
1050	23	21.068	35.2	-16.765
1100	25	23.756	31.0	-16.16
1150	25	23.756	31.0	-15.412
1200	25	23.756	31.0	-14.85
B. For $TiO_{1.98} \pm 0.01$				
1000	45	71.88	9.60	-16.376
1050	45	71.88	9.60	-15.6
1100	53	107.20	6.06	-14.236
1150	53	107.20	6.06	-13.59
1200	53	107.20	6.06	-13.00

Table 4.

Determination of the Power Factor of P_{O_2}

Temperature °C	log $A^{0.5}$ $TiO_{1.98}$	log $A^{0.5}$ $TiO_{1.92}$	log P_{O_2} $TiO_{1.98}$	log P_{O_2} $TiO_{1.92}$	Slopes	x
1000	-1.4265	-1.2140	-16.376	-17.53	$\frac{-0.2125}{1.159} = -0.184$	$-\frac{1}{2.72}$
1050	-1.2880	-1.1275	-15.600	-16.765	$\frac{-0.16}{1.165} = -0.137$	$-\frac{1}{3.65}$
1100	-1.2474	-0.898	-14.236	-16.160	$\frac{-0.35}{1.93} = -0.182$	$-\frac{1}{2.75}$
1150	-1.135	-0.781	-13.590	-15.412	$\frac{-0.354}{1.82} = -0.1825$	$-\frac{1}{2.75}$
1200	-0.287	-0.651	-13.000	-14.850		

Average slope is assumed to be $-\frac{1}{3 \pm 0.65}$

APPENDIX II.

Table 1.

Grain Growth Study

Temperature °C.	Grain Size D μ	Time t min	D^2 μ^2	$D^2 - D_o^2$ μ^2	$t^{0.6}$	log K ($cm^2/min^{0.6}$)
1100	0.73	90	0.5329	0	14.83	(2.15×10^{-10})
(7.35)	0.93	380	0.8649	0.3320	35.4	
	1.40	1055	1.9600	1.4271	65.3	-9.667
	1.66	2555	2.7550	2.2221	110.8	
	2.08	5315	4.3260	3.7031	171.5	
1150	1.365	120	1.8630	1.3301	17.7	(5.8×10^{-10})
(7.12)	1.50	290	2.2500	1.7171	30.2	
	1.91	705	3.6481	3.1152	51.3	-9.237
	2.50	1980	6.2500	5.7171	95.1	
	2.96	3305	8.7616	8.2287	127.2	
	3.34	6605	11.1806	10.5471	197.0	
1200	1.90	110	3.6100	3.0771	16.75	(23.2×10^{-10})
(6.78)	2.57	280	6.6049	6.0720	29.5	
	3.52	1265	12.3904	11.8575	73.0	-8.645
	5.50	2820	30.2500	29.7171	117.3	
	5.93	4183	35.3000	34.9771	149.3	
1250	2.92	100	8.5329	8.0000	15.85	(60×10^{-10})
(6.50)	3.41	240	11.6280	11.0951	26.8	
	5.05	500	25.5329	25.0000	41.7	-8.222
	7.02	1270	49.2800	48.7471	73.3	
	8.60	2620	73.9600	73.4271	112.2	
1300	7.30	90	53.2900	52.7571	14.83	(250×10^{-10})
(6.35)	7.80	150	60.8400	60.3071	20.15	
	12.23	210	149.5300	149.0400	24.80	-7.600
	8.98	250	80.5329	80.0000	27.10	
	9.80	415	96.6400	95.5071	37.15	
	10.30	625	106.0900	105.5570	47.60	

APPENDIX III.

Table 1.

Temp. °C.	Time min.	W gm	$\frac{\Delta W}{W} \times \frac{X}{100}$	O_2 gm	TiO_x	Shrinkage Vol. %	Vol. at Time t cm^3	Weight at Time t gm	Green Bulk Density	Density of Non-stoich. TiO_2	Theo.	$\frac{\rho}{\rho_0}$
1000	0	0.6911	0	0.2771	2	0	4.26	8.3483	1.963	4.25		0.462
	15	0.6905	0.153	0.27615	1.994	6.5	3.98	8.34	2.10	4.244		0.495
	20	0.6893	0.26	0.2753	1.986	9	3.88	8.32	2.15	4.238		0.506
	45				1.986	12	3.75	8.32	2.22	4.238		0.524
	50	0.6879	0.461	0.2739	1.972	16.6	3.55	8.29	2.34	4.227		0.530
	65	0.6876	0.50	0.2760	1.97	9	3.88		2.14	4.225		0.540
	110	0.6866	0.648	0.2726	1.964	12	3.75	8.27	2.222	4.22		0.530
	240	0.68275	1.211	0.26875	1.94	17.2	3.53	8.24	2.34	4.20		0.557
	430	0.6770	2.05	0.2630	1.905	16.8	3.54	8.18	2.34	4.174		0.559
1050	0	0.7500	0	0.3000	2	0	4.26	8.3483	1.97	4.25		0.464
	10	0.7487	0.173	0.2987	1.99	21	3.36	8.33	2.48	4.24		0.587
	15	0.7480	0.27	0.2980	1.986	27.5	3.08	8.315	2.70	4.238		0.636
	35	0.7468	0.43	0.2968	1.98	27.8	3.07	8.31	2.70	4.232		0.632
	75	0.7451	0.646	0.2951	1.968	28.6	3.02	8.28	2.75	4.223		0.650
	100	0.7445	0.74	0.29445	1.964	29.3	3.005	8.280	2.758	4.22		0.654
	240	0.7367	1.77	0.2867	1.92	29.6	2.97	8.225	2.75	4.185		0.656
	1065	0.7360	1.97	0.2880	1.918	30	2.955	8.19	2.78	4.183		0.664
1100	0	0.6909	0	0.2769	2	0	4.28	8.3824	1.96	4.25		0.462
	10		0	0.2769	2	27.8	3.09	8.3824	2.71	4.25		0.638
	10		0	0.2769	2	28.9	3.04	8.3824	2.76	4.25		0.648
	30	0.6876	0.48	0.2736	1.972	32.8	2.88	8.34	2.90	4.226		0.682
	50	0.6856	0.775	0.27165	1.96	35.3	2.77	8.32	3.00	4.217		0.710
	80	0.68399	1.00	0.2699	1.95	35.6	2.76	8.305	3.03	4.209		0.722
	100	0.6828	1.17	0.2688	1.94	37.4	2.69	8.28	3.085	4.201		0.734
	150	0.6808	1.465	0.2668	1.926	37.8	2.67	8.27	3.105	4.19		0.740
	300	0.6790	1.73	0.2650	1.918	38.3	2.65	8.26	3.12	4.183		0.745
	1055	0.67885	1.745	0.26485	1.916	38.5	2.695	8.255	3.125	4.182		0.745

continued...

Table 1.Continued...

Temp. °C.	Time min.	W gm	$\frac{\Delta W}{W} \times \frac{}{100}$	O_2 gm	TiO_x	Shrinkage Vol. %	Vol. at Time t cm^3	Weight at Time t gm	Green Bulk Density	Density of Non-stoichio. TiO_2 Theo.	$\frac{P}{P_0}$
1150	0	0.6663	0	0.2664	2	0	4.28	8.3824	1.94	4.25	
	5	0.6663	0	0.2664	2	35.2	2.78	8.3824	3.02	4.25	0.71
	10	0.6663	0	0.2664	2	36.5	2.725	8.3824	3.08	4.25	0.725
	15	0.66178	0.678	0.26188	1.965	36.5	2.73	8.33	3.06	4.221	0.725
	25	0.66048	0.871	0.26058	1.956	38.3	2.65	8.31	3.14	4.214	0.745
	35	0.6597	0.99	0.2598	1.944	38.3	2.65	8.285	3.13	4.204	0.745
	75	0.65664	1.45	0.25674	1.928	40.6	2.55	8.27	3.25	4.192	0.775
	140	0.65465	1.75	0.25475	1.912	42.5	2.46	8.23	3.345	4.179	0.80
	300	0.65445	1.775	0.25455	1.910	43.7	2.415	8.22	3.405	4.176	0.816
	470	0.65365	1.90	0.25375	1.905	44.0	2.40	8.22	3.425	4.174	0.820
	1065	0.6565	1.90	0.25375	1.905	44.3	2.385	8.22	3.445	4.174	0.825
1200	0	0.8967	0	0.3587	2		4.26	8.3483	1.965	4.25	
	5	0.8967	0	0.3587	2	37.6	2.66	8.3483	3.145	4.25	0.74
	10	0.8912	0.613	0.3532	1.968	38.6	2.61	8.28	3.18	4.224	0.75
	20				1.968	41.8	2.47	8.27	3.345	4.217	0.795
	25	0.88875	0.89	0.35073	1.952			8.255		4.211	
	30					43.0	2.43	8.255	3.40	4.211	0.81
	55	0.8815	1.693	0.3435	1.916	44.2	2.375	8.21	3.46	4.186	0.825
	70	0.8811	1.74	0.3431	1.913	45.8	2.30	8.20	3.565	4.18	0.845
	85					46.0	2.30	8.20	3.57	4.18	0.852
	120	0.8810	1.75	0.3430	1.913	47.4	2.24	8.20	3.665	4.18	0.875
	250	0.8806	1.80	0.3426	1.910	48.2	2.21	8.18	3.71	4.178	0.89
	780	0.8790	1.972	0.3410	1.910	48.6	2.185	8.18	3.75	4.178	0.90

APPENDIX III.

Table 2.

Temp. °C.	Time min	W gm	$\frac{\Delta W}{W} \times \frac{X}{100}$	O_2 gm	TiO_x	Shrinkage Vol. %	Vol. at Time t cm^3	Weight at Time t gm	Green Bulk Density	Density of Non-stoich. TiO_2 Theo.	$\frac{\rho}{\rho_0}$
1000	0	0.8315	0	0.3335	2	0	4.06	8.2556	2.04	4.250	0.480
	20	0.8394	0.132	0.3324	1.994	11	3.61	8.2556	2.29	4.250	0.538
	53	0.8292	0.276	0.3312	1.992	17	3.365	8.245	2.452	4.244	0.578
	113	0.8284	0.376	0.3304	1.984	22.5	3.155	8.24	2.61	4.243	0.616
	233	0.8270	0.542	0.3290	1.974	26	2.995	8.22	2.745	4.236	0.647
	433	0.8270	0.542	0.3290	1.974	24.5	3.055	8.21	2.61	4.228	0.637
	1433	0.8270	0.542	0.3290	1.974	26	2.995	8.22	2.745		0.647
1050	0	0.8444	0	0.3379	2	0	5.44	10.6531	1.96	4.250	0.461
	15	0.84269	0.203	0.33619	1.992	22	4.24	10.62	2.50	4.240	0.588
	27.5	0.84215	0.265	0.33565	1.986	27	3.98	10.62	2.67	4.238	0.630
	55	0.8409	0.415	0.3344	1.984	34	3.60	10.62	2.945	4.236	0.695
	87	0.8403	0.486	0.3338	1.98	37.5	3.36	10.61	3.160	4.234	0.745
	125	0.8401	0.510	0.3336	1.978	38.5	3.333	10.60	3.185	4.231	0.752
	215	0.8401	0.510	0.3336	1.978	39	3.32	10.60	3.19	4.231	0.753
	810	0.8401	0.510	0.3336	1.978	41	3.21	10.60	3.19	4.231	0.743
1100	0	0.8624	0	0.3456	2	0	5.15	9.7650	1.89	4.250	0.445
	10	0.8608	0.186	0.3438	1.99	33	3.80	9.7645	2.57	4.248	0.606
	15	0.8604	0.225	0.3436	1.985	32	3.58	9.7645	2.74	4.248	0.646
	35	0.8595	0.340	0.3427	1.98	36	3.30	9.7645	2.96	4.248	0.696
	55	0.8580	0.510	0.3410	1.976	40	3.09	9.726	3.15	4.230	0.743
	105	0.8577	0.545	0.3407	1.972	44	2.88	9.7	3.37	4.227	0.795
	490	0.8566	0.573	0.3396	1.970	45	2.82	9.7	3.44	4.225	0.815
	1075	0.8566	0.573	0.3396	1.970	45.5	2.80	9.7	3.46	4.225	0.818
	2336	0.8566	0.573	0.3396	1.970	45.5	2.80	9.7	3.46	4.225	0.818
	3650	0.8566	0.573	0.3396	1.970	46	2.78	9.7	3.49	4.225	0.827
	5121	0.8566	0.573	0.3396	1.970	46	2.78	9.7	3.49	4.225	0.827
	9910	0.8566	0.573	0.3396	1.970	46	2.78	9.7	3.49	4.225	0.827

continued...

Table 2. Continued...

Temp. °C.	Time min.	W gm	$\frac{\Delta W}{W} \times 100$	O_2 gm	TiO_x	Shrinkage Vol. %	Vol. at Time t cm^3	Weight at Time t gm	Green Bulk Density	Density of Non-stoich. TiO_2 Theo.	$\frac{\rho}{\rho_0}$
1150	0	0.8832	0	0.3532	2	0	5.41	10.5365	1.95	4.25	0.458
	15	0.8802	0.310	0.3502	1.986	38.2	3.34	10.51	3.14	4.248	0.74
	45	0.8789	0.487	0.3489	1.978	40.0	3.245	10.48	3.23	4.226	0.764
	105	0.8783	0.555	0.3483	1.974	41.8	3.14	10.48	3.345	4.225	0.792
	275	0.8780	0.590	0.3480	1.972	45.0	2.98	10.48	3.52	4.228	0.833
	2555	0.8775	0.645	0.3475	1.97	50	2.705	10.47	3.87	4.225	0.915
	4440	0.8775	0.645	0.3475	1.97	50	2.705	10.47	3.87	4.225	0.915
1200	0	1.7234	0	0.6874	2	0	4.80	9.5779	1.995	4.25	0.469
	22	1.7209	0.140	0.6849	1.99	39	2.99	9.5779	3.21	4.24	0.755
	30	1.7190	0.255	0.6830	1.988	41	2.84	9.56	3.37	4.24	0.793
	38	1.7168	0.380	0.6808	1.980	43	2.73	95.3	3.50	4.235	0.825
	60	1.7142	0.534	0.6782	1.976	47	2.53	95.2	3.85	4.23	0.87
	125	1.7142	0.534	0.6782	1.976	49.5	2.43	95.2	3.92	4.23	0.925
	245	1.7142	0.534	0.6782	1.976	49.5	2.43	95.2	3.92	4.23	0.925
	755	1.7142	0.534	0.6782	1.976	49.5	2.43	95.2	3.92	4.23	0.225
	1075	1.7142	0.534	0.6782	1.976	49.6	2.42	95.2	3.94	4.23	0.93
	2035	1.7142	0.534	0.6782	1.976	49.6	2.42	95.2	3.94	4.23	0.93
	3415	1.7142	0.534	0.6782	1.976	49.6	2.42	95.2	3.94	4.23	0.93

Table 3.

Data for Diffusion Coefficient Calculation for the Final Composition of $TiO_{1.92}$

Temperature °C	D μ	D^3 μ^3	t min.	$A(T)\frac{cm^3}{sec}$	log A(T)
1100	0.73	0.389	90	3.13×10^{-17}	-16.505
(7.35)	0.93	0.8044	380		
	1.40	2.744	1055		
	1.66	4.5733	2555		
	2.08	8.998	5315		
1150	1.365	2.5432	120	1.27×10^{-16}	-15.8955
(7.12)	1.50	3.375	290		
	1.91	6.968	705		
	2.50	15.625	1980		
	2.96	25.934	3305		
	3.34	37.260	6605		
1200	1.90	6.859	110	8.25×10^{-16}	-15.085
(6.78)	2.57	16.9745	280		
	3.52	43.613	1265		
	5.50	16.640	2820		
	5.93	208.530	4183		
1250	2.92	25.020	100	4.25×10^{-15}	-14.37
(6.56)	3.41	39.6514	240		
	5.05	128.500	500		
	7.02	345.945	1270		
	8.60	636.056	2620		
1300	7.30	389.017	90	3.67×10^{-14}	-13.4355
(6.35)	7.80	474.552	150		
	12.23		210		
	8.92	708.000	250		
	9.80	941.190	415		
	10.30	1092.727	625		
1000				8.12×10^{-19}	-18.09
(7.94)					
1050				4.36×10^{-18}	-17.36
(7.67)					

Table 4.

Diffusion Coefficient Calculations for the Final Composition of $TiO_{1.92}$

Temperature °C.	A(T) $\frac{cm^3}{sec}$	Slopes $\left(\frac{P}{P_0}\right)$ / log t	$D = -\frac{\text{Slope } A\ T}{2.62 \times 10^{-3}}$	log D
1000 (7.94)	8.12×10^{-19}	5.6×10^{-2}	2.21×10^{-14}	-13.656
1050 (7.67)	4.36×10^{-18}	6×10^{-2}	1.325×10^{-13}	-12.878
1100 (7.35)	3.13×10^{-17}	6×10^{-2}	9.77×10^{-13}	-12.011
1150 (7.12)	1.27×10^{-16}	6.1×10^{-2}	4.22×10^{-12}	-11.3755
1200 (6.78)	8.25×10^{-16}	9.3×10^{-2}	4.32×10^{-11}	-10.366

Table 5.

Data for Diffusion Coefficient Calculations for $TiO_{1.98}$ and TiO_2 at 1200°C

Final Composition	Time min.	D μ	D^3 μ^3	K $\frac{cm^3}{sec}$
$TiO_{1.98}$	290	2.16	14.743	4.53×10^{-16}
	2625	4.50	91.125	
	5625	5.26	145.528	
TiO_2	354	1.92	7.0779	7.94×10^{-16}
	489	2.26	11.5432	
	1414	4.20	74.01	
	2790	5.10	132.20	
	10640	12.5	1953.125	

Table 6.

Diffusion Coefficient Calculations at 1200°C

Final Domposition	K $\frac{cm^3}{sec}$	Slopes $(\frac{1}{min})$	D $= \frac{\text{Slope K T}}{2.623 \times 10^{-3}}$ $\frac{cm^2}{sec}$
$TiO_{1.98}$	4.53×10^{-16}	0.23	5.86×10^{-11}
TiO_2	7.94×10^{-16}	0.27	12.51×10^{-11}

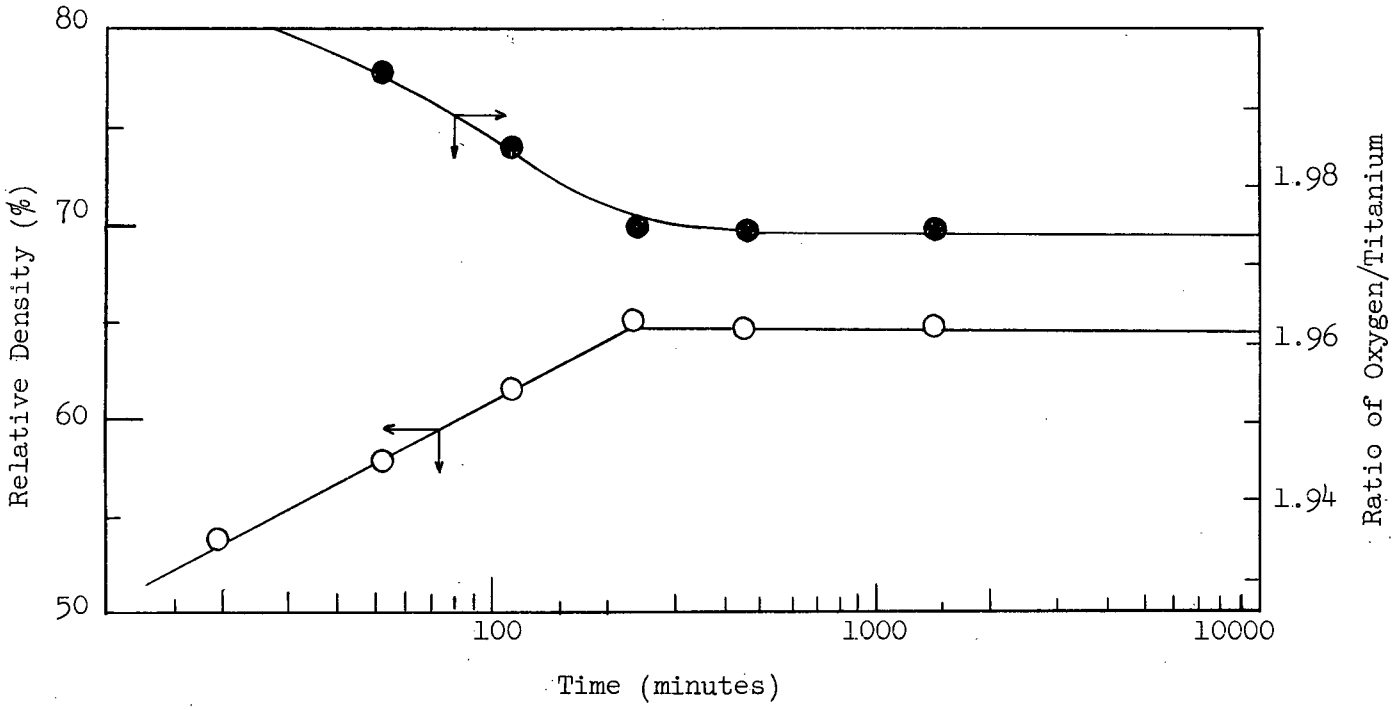

Figure A.III-1a. Densification of Compacts for the Final Composition of $TiO_{1.98}$ at T = 1000°C.

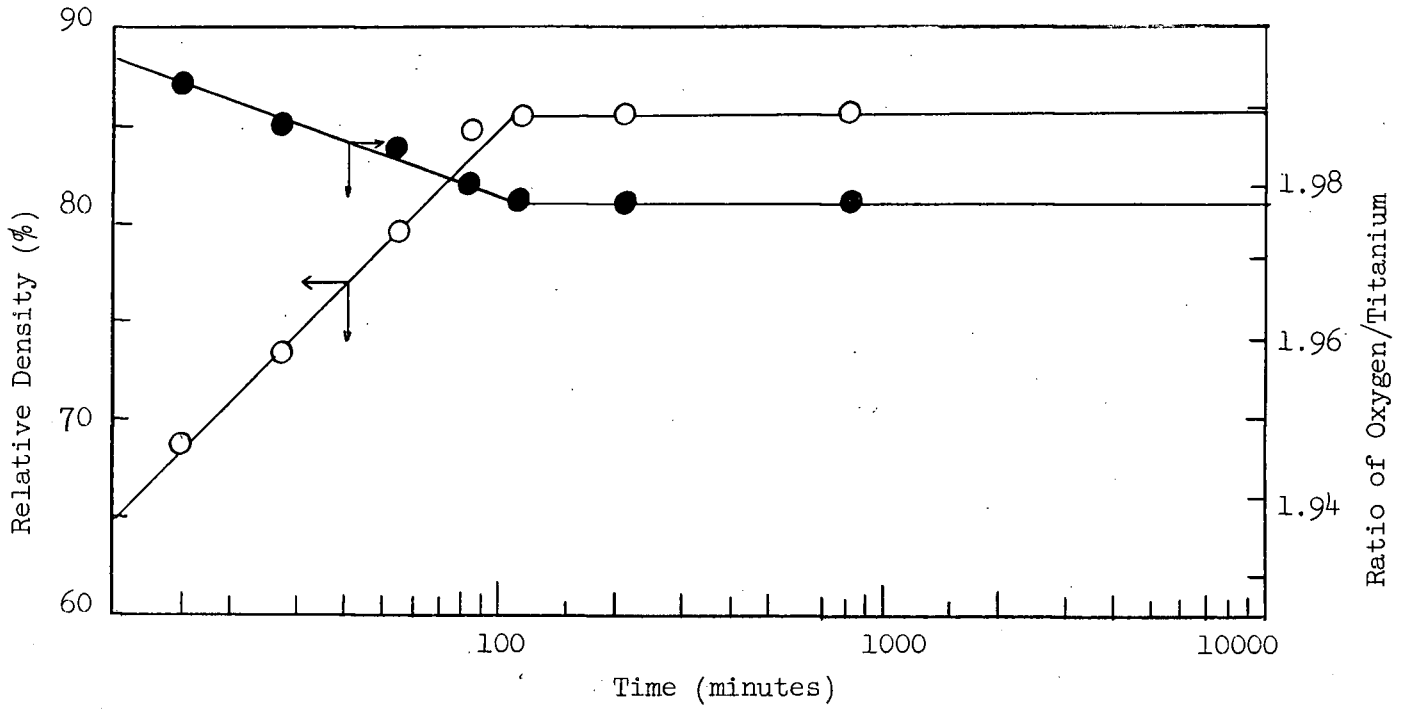

Figure A.III-1b. Densification of Compacts for the Final Composition of $TiO_{1.98}$ at T = 1050°C.

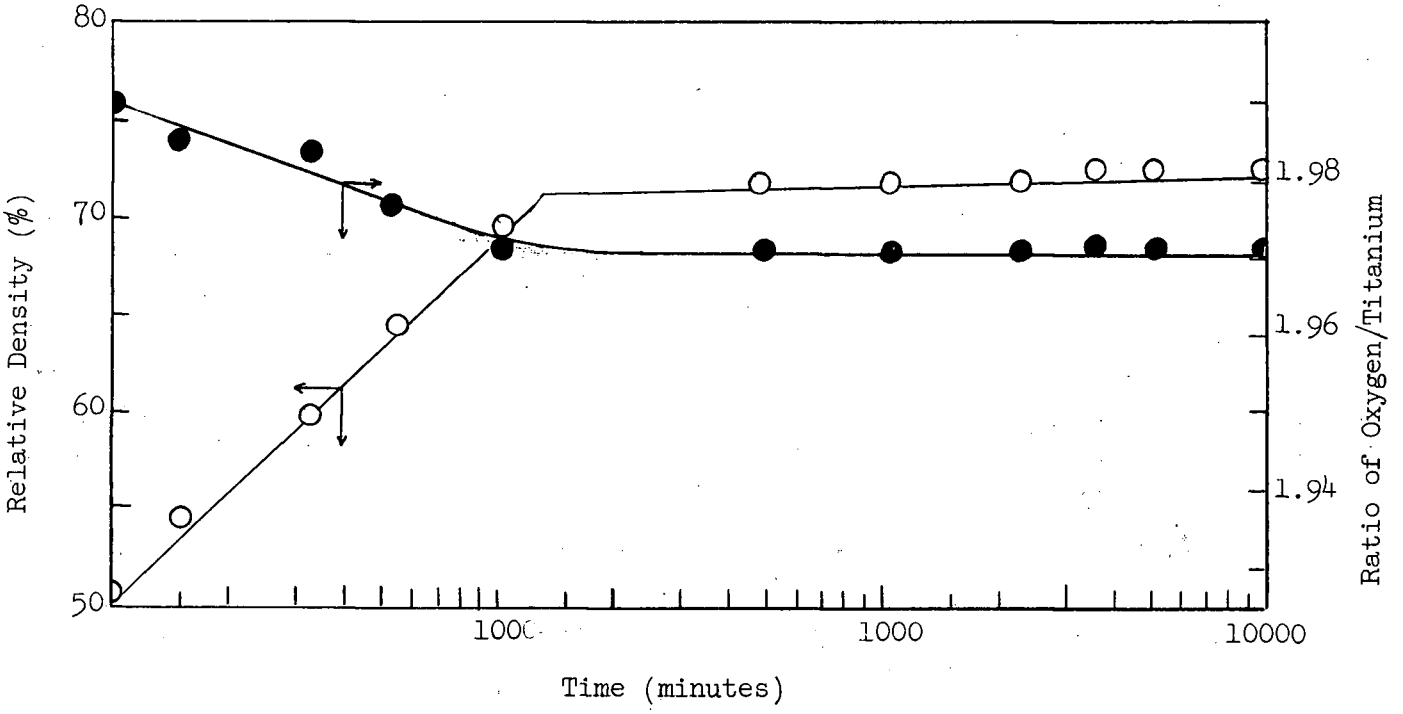

Figure A.III-1c. Densification of Compacts for the Final Composition of $TiO_{1.98}$ at T = 1100°C.

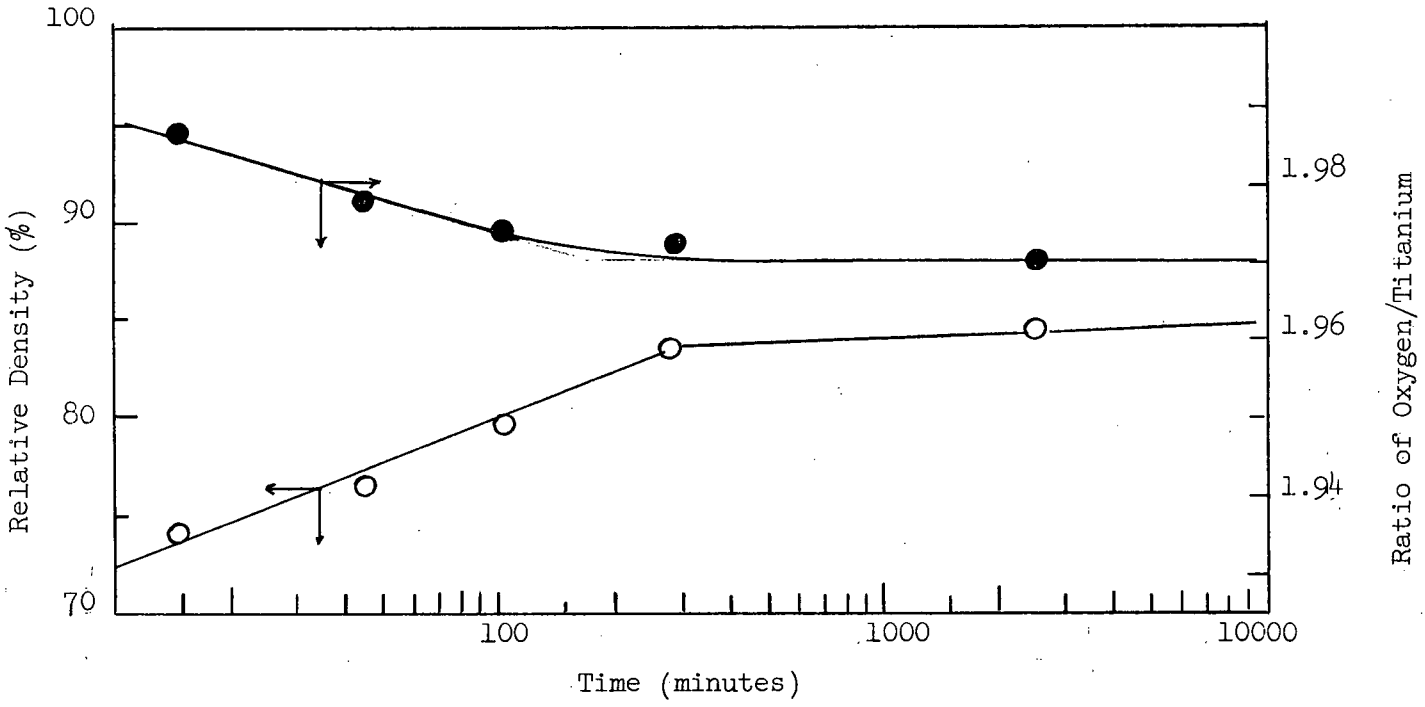

Figure A.III-1d. Densification of Compacts for the Final Composition of $TiO_{1.98}$ at T = 1150°C.

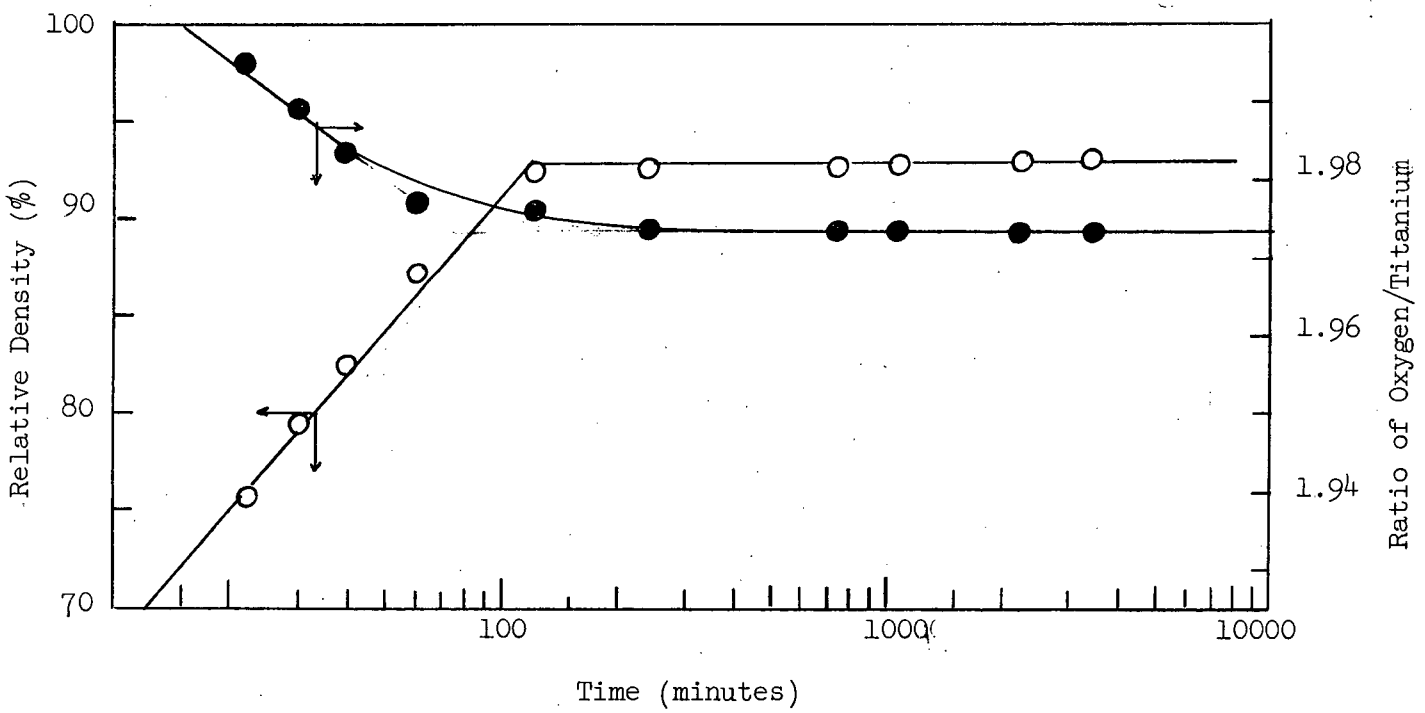

Figure A.III-1e. Densification of Compacts for the Final Composition of $TiO_{1.98}$ at T = 1200°C.

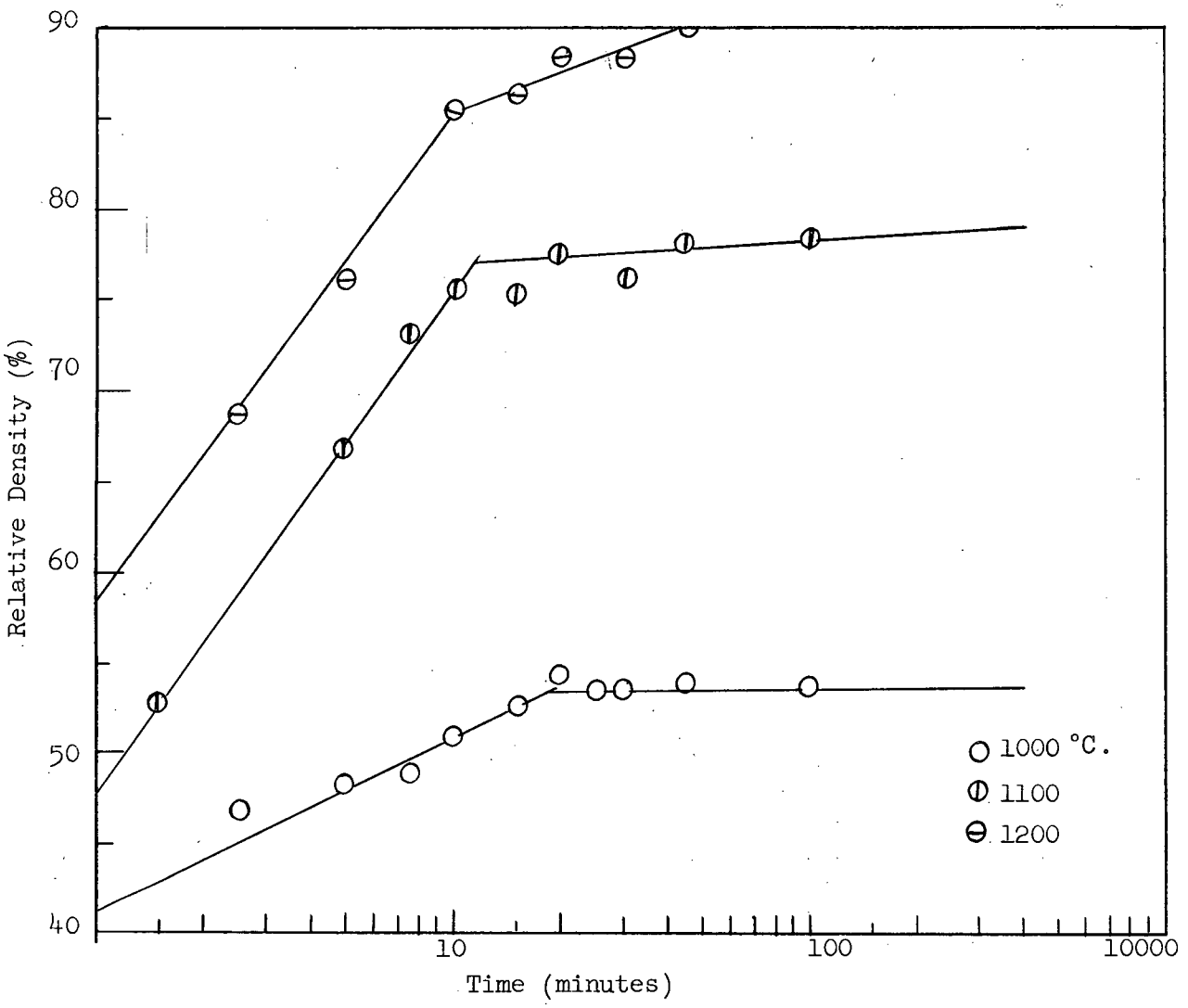

Figure A.III-2. Densification of Compacts of Stoichiometric Rutile TiO_2 at Different Temperatures.

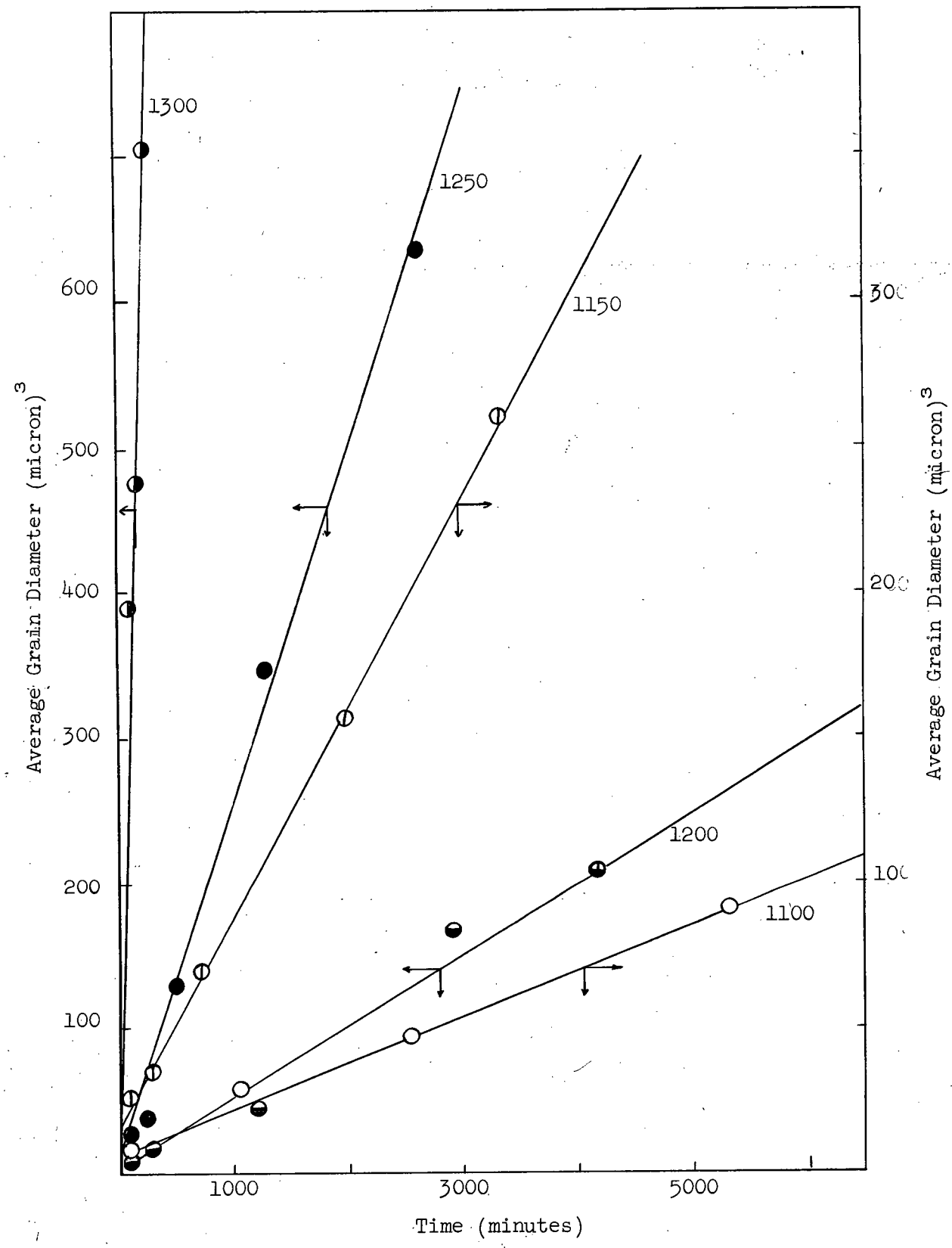

Figure A.III-3 Variation of Grain Size with Time and Temperature. This is to determine A of equation (16).

APPENDIX IV.

Defect Equilibria and Oxygen Ion Diffusion for Non-Stoichiometric Rutile

If the diffusion rate constants for both O^{2-} and $V_{O^{2-}}$ are measured independently as functions of temperature, the heat of vacancy formation and the concentration of vacancies at different temperatures can be determined by the relationship

$$D_{O^{2-}} \times [O^{2-}] = D_{V_{O^{2-}}} \times [V_{O^{2-}}]$$

where D indicates the diffusion constants of the respective species. On simplifying and noting that $[O^{2-}]$ in the lattice is almost unity,

$$D_{O^{2-}} \simeq D_{V_{O^{2-}}} [V_{O^{2-}}]$$

$$= \nu a^2 [V_{O^{2-}}] \exp\left(-\frac{U}{KT}\right)$$

where ν is the vibrational frequency of oxygen ion and a, is the distance between adjacent oxygen ions, U the activation energy for the motion of an oxygen vacancy through the lattice.

Substituting the vacancy concentration $[V_{O^{2-}}]$ of equation (21) the diffusion coefficient $D_{O^{2-}}$ is:

$$D_{O^{2-}} = C_{PO_2}^{-1/6} \nu a^2 \exp\left[-\frac{\Delta H_f^\circ}{3RT} - \frac{U}{RT}\right] = C'_{PO_2}^{-1/6} \exp\left[-\left(\frac{\Delta H_f^\circ}{3RT} + \frac{U}{RT}\right)\right]$$

where $C' = C \nu a^2$.

This equation can be further simplified by using the usual frequency factor D_o

$$D_{O^{2-}} = D_o \exp -\left(\frac{\Delta H_f^\circ}{3RT} + \frac{U}{RT}\right).$$

It is significant to note that the frequency factor in this equation depends on $PO_2^{-1/6}$ and this expression for the oxygen ion diffusion coefficient is valid only at high temperatures, so that virtually all the vacancies are completely ionized.

APPENDIX V

Boundary Diffusion Model (Coble[5])

$$P = \left[\frac{2D_b W \gamma a_o^3}{l^4 k T} t \right]^{2/3}$$

$$l^4 = D^4 = A(T)\, t$$

$$\frac{dP^{3/2}}{dt} = \frac{2D_b W \gamma a_o^3}{A k T} \cdot \frac{1}{t}$$

$$\left[P^{3/2} \right]_{P_0}^{0} = \frac{2D_b W \gamma a_o^3}{A k T} \left[\ln t \right]_{o}^{t}$$

A plot of D^4 versus time produced the values of A shown in the Appendix V, Table 1. and a plot of $\left(\frac{P}{P_0}\right)^{3/2}$ versus log t produced the slopes S at different temperatures. Using the following known value of the constants the values of D_b of different temperature are calculated and shown in Appendix V, Table 1.

D_b = boundary diffusion coefficient cm^2/sec

γ = 10^3 ergs/cm^3

a_o^3 = 1.57×10^{-23} cm^3

k = 1.38×10^{-16} ergs/deg

W = 25 Å

APPENDIX V.

Table 1.

Temperature °C.	Time min.	D^2 μ^2	D^4 μ^4	A(T) $\frac{cm^4}{sec}$	Slope S	D_b = (S) AT 1.76×10^{-10} $\frac{cm^2}{sec}$	log D_b
1100	90	0.5329	0.283	5.7×10^{-21}	0.101	1.391×10^{-8}	-7.856
(7.35)	380	0.8649	0.748				
	1055	1.96	3.85				
	2555	2.755	7.55				
	5315	4.326	19.7				
1150	120	1.863	3.47	3.3×10^{-20}	0.082	6.77×10^{-8}	-7.1695
(7.12)	290	2.25	5.1				
	705	3.65	13.3				
	1980	6.25	39				
	3305	8.76	77				
	6605	11.18	125				
1200	110	3.61	13	5.0×10^{-19}	0.132	1.71×10^{-6}	-5.767
(6.78)	280	6.6	43.5				
	1265	12.4	154				
	2820	30.25	915				
	4183	35.3	1245				
1250	240	11.628	135	3.1×10^{-18}			
(6.56)	1270	49.3	2420				
	2620	74.0	5480				
1300	90	53.3	2820	—			
	150	60.8	3720				
	210	150.0					
	415	96.0	9200				
	625	106.0	11200				
1000				5.75×10^{-23}	0.045	5.8×10^{-11}	-10.237
(7.94)							
1050				4.56×10^{-22}	0.073	7.74×10^{-10}	-9.112
(7.67)							

THE UNIVERSITY OF BRITISH COLUMBIA

VANCOUVER 8, CANADA

DEPARTMENT OF METALLURGY

Comments on Thesis and Oral Examination Of

Jacques Pierre Jean Thiriar

"SINTERING AND GRAIN GROWTH OF NON-STOICHIOMETRIC RUTILE"

This thesis was subjected to criticism due to the treatment of activation energies and their calculations. The anomaly is in the use of a rate constant for Arrhenius plots that involves time to a power other than unity.

On page 29, Figure 12 the plots are for weight loss in terms of log $(\frac{1}{min})^{1/2}$ versus 1/T and the slopes correspond to approximately 42 kilocalories on these plots. The quoted activation energy at the top of page 30 is 82 ± 2 kilocalories per mole which indicates that the author has doubled the value in recognition of the effect of using a 1/2 power in the time unit of his rate function. This treatment is justifiable since a true rate law based on fundamental mechanisms has not yet been obtained at this point.

On page 36, Figure 17 the plot is for grain growth and uses a rate function of dimension $(\frac{cm^2}{min})^{0.6}$. The slope is estimated at 80 kilocalories from this slope. The activation energy quoted by the author for this is 78 kilocalories per mole (page 32 line 13 of the first paragraph) which indicates that no correction for the time function has been made in this case. This is not justifiable since the Arrhenius law is based upon a plot of a fundamental rate constant and the time exponent is always -1 regardless of reaction order or complexity of the rate law. Time exponents of other value may be used when the rate law is not really known, but the activation energy must be corrected by dividing it by the time exponent. In this case the activation energy is $78/_{0.6}$ or 130 kilocalories per mole.

Arrhenius plots are again shown on page 43 Figure 19 and use a unit time dimension in the rate constant. This should yield valid activation energy values.

The author has used certain procedures apparently accepted in the ceramics literature in his treatment of Figure 17 and should therefore not be condemned, but the procedure is recognizably wrong to those familiar with the fundamentals of kinetics processes. It is probable that many erroneous conclusions regarding mechanisms in solid state kinetic processes have been drawn from the use of this procedure, and it is recommended that attempts be made to correct them in future studies where this erroneous procedure may normally be applied.

E. Peters,
Associate Professor.

EP/jmk
March 3, 1964